optica

Controlling phonons and photons at the wavelength scale: integrated photonics meets integrated phononics

Amir H. Safavi-Naeini,[1] Dries Van Thourhout,[2] Roel Baets,[2] and Raphaël Van Laer[1,2,*]

[1]Department of Applied Physics and Ginzton Laboratory, Stanford University, Stanford, California 94305, USA
[2]Photonics Research Group (INTEC), Department of Information Technology, Ghent University–imec, Belgium
Center for Nano- and Biophotonics, Ghent University, Ghent, Belgium
*Corresponding author: rvanlaer@stanford.edu

Received 25 September 2018; revised 11 December 2018; accepted 16 January 2019 (Doc. ID 346672); published 19 February 2019

Radio-frequency communication systems have long used bulk- and surface-acoustic-wave devices supporting ultrasonic mechanical waves to manipulate and sense signals. These devices have greatly improved our ability to process microwaves by interfacing them to orders-of-magnitude slower and lower-loss mechanical fields. In parallel, long-distance communications have been dominated by low-loss infrared optical photons. As electrical signal processing and transmission approach physical limits imposed by energy dissipation, optical links are now being actively considered for mobile and cloud technologies. Thus there is a strong driver for wavelength-scale mechanical wave or "phononic" circuitry fabricated by scalable semiconductor processes. With the advent of these circuits, new micro- and nanostructures that combine electrical, optical, and mechanical elements have emerged. In these devices, such as optomechanical waveguides and resonators, optical photons and gigahertz phonons are ideally matched to one another, as both have wavelengths on the order of micrometers. The development of phononic circuits has thus emerged as a vibrant field of research pursued for optical signal processing and sensing applications as well as emerging quantum technologies. In this review, we discuss the key physics and figures of merit underpinning this field. We also summarize the state of the art in nanoscale electro- and optomechanical systems with a focus on scalable platforms such as silicon. Finally, we give perspectives on what these new systems may bring and what challenges they face in the coming years. In particular, we believe hybrid electro- and optomechanical devices incorporating highly coherent and compact mechanical elements on a chip have significant untapped potential for electro-optic modulation, quantum microwave-to-optical photon conversion, sensing, and microwave signal processing.

https://doi.org/10.1364/OPTICA.6.000213

1. INTRODUCTION

Microwave-frequency acoustic or mechanical wave devices have found numerous applications in radio-signal processing and sensing. They already form mature technologies with large markets, typically exploited for their high quality compared to electrical devices [1]. The vast majority of these devices are made of piezoelectric materials that are driven by electrical circuits [2–8]. A major technical challenge in such systems is obtaining the suitable matching conditions for efficient conversion between electrical and mechanical energy. Typically, this entails reducing the effective electrical impedance of the electromechanical component by increasing the capacitance of the driving element. This has generally led to devices with large capacitors that drive mechanical modes with large mode volumes. Here, we describe a recent shift in research toward structures that are only about a wavelength, i.e., roughly 1 μm at gigahertz frequencies, across in two or more dimensions.

Greater confinement of mechanical waves in a device has both advantages and drawbacks, depending on the application at hand. In the case of interactions with optical fields, higher confinement increases the strength and speed of the interaction, allowing faster switching and lower powers. A smaller system demands less dissipated energy to achieve the same effects, simply because it focuses all of the optical and mechanical energy into a smaller volume. High confinement also enables scalable, less costly fabrication with more functionality packed into a smaller space. Perhaps more importantly, in analogy to microwave and photonic circuits that become significantly easier to engineer in the single- and few-moded limits, obtaining control over the full mode structure of the devices vastly simplifies designing and scaling systems to higher complexity. Confining mechanical energy is not without its drawbacks; as we will see below, focusing the mechanical energy into a small volume also means that deleterious nonlinear effects manifest at lower powers, and matching directly to

Corrected 19 February 2019

microwave circuits becomes significantly more difficult due to vanishing capacitances. We can classify confinement in terms of its dimensionality (Fig. 1). The dimensionality refers to the number of dimensions where confinement is on the scale of the wavelength of the excitation in bulk. For example, surface acoustic wave (SAW) resonators [2], much like thin-film bulk acoustic wave (BAW) resonators [3], have wavelength-scale confinement in only one dimension—perpendicular to the chip surface—and are therefore 1D-confined. Until a few years ago, wavelength-scale phononic confinement at gigahertz frequencies beyond 1D remained out of reach.

Intriguingly, both near-infrared optical photons and gigahertz phonons have a wavelength of about 1 μm. This results from the 5 orders of magnitude difference in the speed of light relative to the speed of sound. The fortuitous matching of length scales was used to demonstrate the first 2D- and 3D-confined systems, in which both photons and phonons are confined to the same area or volume (Fig. 1). These measurements have been enabled by advances in low-loss photonic circuits that couple light to material deformations through boundary and photoelastic perturbations. Direct capacitive or piezoelectric coupling to these types of resonances has been harder, since the relatively low speed of sound in solid-state materials means that gigahertz-frequency phonons have very small volume, leading to minuscule electrically induced forces at reasonable voltages, or, in other words, large motional resistances that are difficult to match to standard microwave circuits [1].

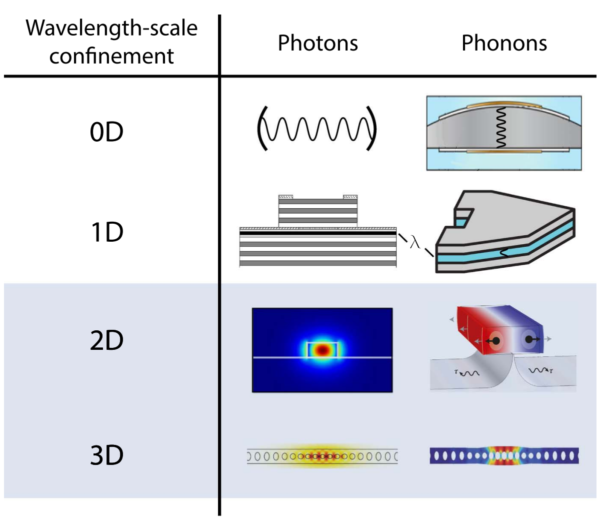

Fig. 1. Confining photons and phonons to the wavelength-scale. Photonic and phononic systems can be classified according to the number of dimensions in which they confine excitations to a wavelength. Most previous systems contain several wavelengths in more than one dimension: they are 0D- or 1D-confined. New structures have emerged in which both photons and phonons are confined to the wavelength scale in two or three dimensions. Here we focus on such 2D- or 3D-confined wavelength-scale systems at gigahertz frequencies. Related reviews on integrated opto- and electromechanical systems are [9,17,31,33,45,113,183,205,206]. The table gives as examples of 2D- and 3D-confined devices a sub-μm^2 silicon photonic-phononic waveguide [34] and a sub-μm^3 silicon optomechanical crystal [114]. The depicted 0D- and 1D-confined structures are a long Fabry–Perot cavity, a vertical-cavity surface-emitting laser [20] for the optical case and a thick quartz [21] and a thin aluminum nitride BAW resonator [177] for the mechanical case. The study of heat flow [23,45] is beyond the scope of this review.

Here, we primarily consider recent advances in gigahertz-frequency *phononic* devices. These devices have been demonstrated mainly in the context of photonic circuits and share many commonalities with integrated photonic structures in terms of their design and physics. They also have the potential to realize important new functionalities in photonic circuits. Despite recent demonstrations of confined mechanical devices operating at gigahertz frequencies and coupled to optical fields, phononic circuits are still in their infancy, and applications beyond those of interest in integrated photonics remain largely unexplored. Several attractive aspects of mechanical elements remain unrealized in chip-scale systems, especially in those based on nonpiezoelectric materials.

In this review, we first describe the basic physics underpinning this field, with specific attention to the mechanical aspects of optomechanical devices. We discuss common approaches used to guide and confine mechanical waves in nanoscale structures in Section 2. Next, we describe the key mechanisms behind interactions between phonons and both optical and microwave photons in Section 3. These interactions allow us to efficiently generate and readout mechanical waves on a chip. Section 4 briefly summarizes the state of the art in opto- and electromechanical devices. It also describes a few commonly used figures of merit in this field. Finally, we give our perspectives on the field in Section 5. In analogy to integrated photonics [10–16,18,19,22,24,25], the field may be termed "integrated *phononics*." While not limited to the material silicon, its goal is to develop a platform whose fabrication is in principle scalable to many *densely integrated* and *coherent* phononic devices.

2. GUIDING AND CONFINING PHONONS

Phonons obey broadly similar physics as photons so they can be guided and confined by comparable mechanisms, as detailed in the following subsections.

A. Total Internal Reflection

In a system with continuous translational symmetry, waves incident on a medium totally reflect when they are not phase-matched to any excitations in that medium. This is called total internal reflection. The waves can be confined inside a slow medium sandwiched between two faster media by this mechanism [Fig. 2(a)]. This ensures that at fixed frequency Ω the guided wave is not phase-matched to any leaky waves since its wave vector $K(\Omega) = \Omega/v_\phi$—with v_ϕ its phase velocity—exceeds the largest wave vector among waves in the surrounding media at that frequency. In other words, the confined waves must have maximal slowness $1/v_\phi$. This principle applies to both optical and mechanical fields [26–28].

Still, there are important differences between the optical and mechanical cases. For instance, a bulk material has only two transverse optical polarizations while it sustains two transverse mechanical polarizations with speed v_t and a longitudinally polarized mechanical wave with speed v_l. Unlike in the optical case, these polarizations generally mix in a complex way at interfaces [26]. In addition, a boundary between a material and air leads to geometric softening (see next section), a situation in which interfaces reduce the speed of certain mechanical polarizations. This generates slow SAW modes that are absent in the optical case. So achieving mechanical confinement requires care in looking

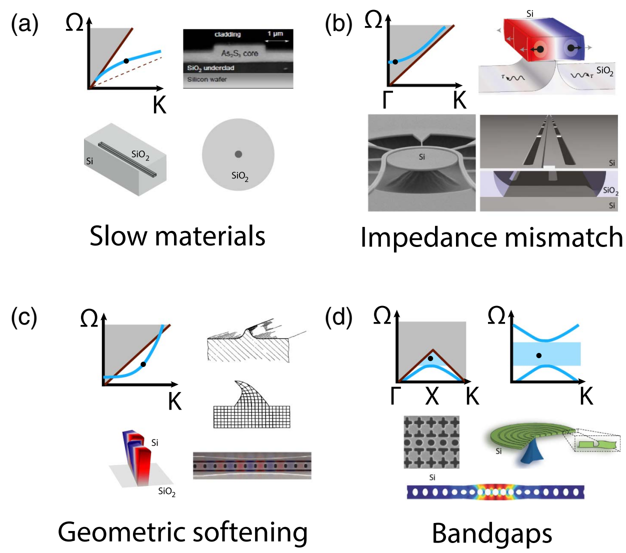

Fig. 2. Mechanisms for phononic confinement in micro- and nanostructures. We illustrate the main approaches with phononic dispersion diagrams $\Omega(K)$ and mark the operating point in black. (a) A waveguide core whose mechanical excitations propagate more slowly than the slowest waves in the surrounding materials supports acoustic total internal reflection. Examples include chalcogenide rib waveguides on silica [31], silica waveguides cladded by silicon [29], and Ge-doped fibers [30]. (b) Even when phonons are phase-matched to surface or bulk excitations, their leakage can be limited by impedance mismatch such as in suspended silicon waveguides and disks [34–36,42,44] and silica microtoroids [115]. (c) In contrast to optical fields, mechanical waves can be trapped by surface perturbations that soften the elastic response such as in case of Rayleigh surface waves [2], silicon fins on silica [40,41], and all-silicon surface perturbations [37–39,51]. (d) Finally, phonons can be trapped to line or point defects in periodic structures with a phononic bandgap such as in silicon optomechanical crystals [52,114], line defects [57], and bulls-eye disks [54]. Many structures harness a combination of these mechanisms.

for the slowest waves in the surrounding structures. These are often surface instead of bulk excitations. Among the bulk excitations, transversely polarized phonons are slower than longitudinally polarized phonons ($v_t < v_l$).

Conflicting demands often arise when designing waveguides or cavities to confine photons and phonons in the same region: photons can be confined easily in dense media with a high refractive index and thus small speed of light, but phonons are naturally trapped in soft and light materials with a small speed of sound. In particular, the mechanical phase velocities scale as $v_\phi = \sqrt{E/\rho}$, with E the stiffness or Young's modulus and ρ the mass density. For instance, a waveguide core made of silicon (refractive index $n_{Si} = 3.5$) and embedded in silica ($n_{SiO_2} = 1.45$) strongly confines photons by total internal reflection but cannot easily trap phonons (for exceptions see next sections). On the other hand, a waveguide core made of silica ($v_t = 5500$ m/s) embedded in silicon ($v_t = 5843$ m/s) can certainly trap mechanical [29] but not optical fields. Still, some structures find a sweet spot in this trade-off: the principle of total internal reflection is currently exploited to guide phonons in Ge-doped optical fibers [30] and chalcogenide waveguides [31].

Since silicon is "slower" than silicon dioxide optically, but "faster" acoustically, simple index guiding for co-confined optical and mechanical fields is not an option in the canonical platform of silicon photonics, silicon-on-insulator. Below we consider techniques that circumvent this limitation and enable strongly co-localized optomechanical waves and interactions.

B. Impedance Mismatch

The generally conflicting demands between photonic and phononic confinement (see above) can be reconciled through impedance mismatch [Fig. 2(b)]. The characteristic acoustic impedance of a medium is $Z_m = \rho v_\phi$, with ρ the mass density [26]. Interfaces between media with widely different impedances Z_m, such as between solids and gases, strongly reflect phonons. In addition, gases have an acoustic cutoff frequency—set by the molecular mean-free path—above which they do not support acoustic excitations [32]. At atmospheric pressure, this frequency is roughly $\Omega_c/(2\pi) \approx 0.5$ GHz. Above this frequency Ω_c acoustic leakage and damping because of air are typically negligible. The cutoff frequency Ω_c can be drastically reduced with vacuum chambers, an approach that has been pursued widely to confine low-frequency phonons [33]. These ideas were harnessed in silicon-on-insulator waveguides to confine both photons and phonons to silicon waveguide cores [34–36] over milli- to centimeter propagation lengths. The acoustic impedances of silicon and silica are quite similar, so in these systems the silica needs to be removed to realize low phonon leakage from the silicon core. In one approach [34], the silicon waveguide was partially underetched to leave a small silica pillar that supports the waveguide [Fig. 2(b)]. In another, the silicon waveguide was fully suspended while leaving periodic silica or silicon anchors [35,36].

C. Geometric Softening

The guided wave structures considered above utilize full or partial underetching of the oxide layer to prevent leakage of acoustic energy from the silicon into the oxide. Geometric softening is a technique that allows us to achieve simultaneous guiding of light and sound in a material system without underetching and regardless of the bulk wave velocities. Although phonons and photons behave similarly in bulk media, their interactions with boundaries are markedly different. In particular, a solid-vacuum boundary geometrically softens the structural response of the material below and thus lowers the effective mechanical phase velocity [Fig. 2(c)]. This is the principle underpinning the 1D confinement of Rayleigh SAWs [26,37]. This mechanism was used in the 1970s in the megahertz range [37–39] to achieve 2D confinement and was recently rediscovered for gigahertz phonons, where it was found that both light and motion can be guided in unreleased silicon-on-insulator structures [40]. More recently, fully 3D-confined acoustic waves have been demonstrated [41] with this approach on silicon-on-insulator where a narrow silicon fin, clamped to a silicon dioxide substrate, supports both localized photons and phonons.

D. Phononic Bandgaps

Structures patterned periodically, such as a silicon slab with a grid of holes, with a period a close to half the phonons' wavelength $\Lambda = 2\pi/K$ result in strong mechanical reflections, as in the optical case. At this X-point—where $K = \pi/a$—in the dispersion diagram forward- and backward-traveling phonons are strongly coupled, resulting in the formation of a phononic bandgap [Fig. 2(d)] whose size scales with the strength of the periodic perturbation. The states just below and above the bandgap can be tuned by locally and smoothly modifying geometric properties of the lattice, resulting in the formation of line or point defects. This technique is pervasive in photonic crystals [43] and was adapted to the mechanical case in the last decade [45–50]. This led to the demonstration of optomechanical crystals that 3D-confine both photons and gigahertz phonons to wavelength-scale suspended silicon nanobeams [52,53,55]. In these experiments, confinement in one or two dimensions was obtained by periodic patterning of a bandgap structure, while in the remaining dimension, confinement is due to the material being removed to obtain a suspended beam or film.

Conflicting demands similar to those discussed in Section 2.B complicate the design of *simultaneous* photonic-phononic bandgap structures [50]. For example, a hexagonal lattice of circular holes in a silicon slab, as is often used in photonic bandgap cavities and waveguides, does not lead to a full phononic bandgap. Conversely, a rectangular array of cross-shaped holes in a slab, as has been used to demonstrate full phononic bandgaps in silicon and other materials, does not support a photonic bandgap. Nonetheless, both one-dimensional [55] and two-dimensional crystals [52] with simultaneous photonic and phononic gaps have been proposed and demonstrated in technologically relevant material systems. In addition, full bandgaps are ideal [56] but not strictly necessary for good confinement as long as there is strong reflectivity within the momentum-distribution associated with the confined excitations and the disorder [43].

Beyond enabling 3D-confined wavelength-scale phononic cavities, phononic bandgaps also support waveguides or wires, which are 2D-confined defect states. These have been realized in silicon slabs with a pattern of cross-shaped holes supporting a full phononic bandgap, with an incorporated line defect within the bandgap material [57–60]. Robustness to scattering is particularly important to consider in such nano-confined guided wave structures, since as in photonics, intermodal scattering due to fabrication imperfections increases with decreasing cross-sectional area of the guided modes [61]. Single-mode phononic wires are intrinsically more robust, as they remove all intermodal scattering except backscattering. They have been demonstrated to allow robust and low-loss phonon propagation over millimeter-length scales [60]. Multi- and single-mode phononic waveguides are currently considered as a means of generating connectivity and functionality in chip-scale solid-state quantum emitter systems using defects in diamond [62,63].

E. Other Confinement Mechanisms

The above mechanisms for confinement cover many, if not most, current systems. However, there are alternative mechanisms for photonic and phononic confinement, including but not limited to: bound states in the continuum [64–66], Anderson localization [67,68], and topological edge states [69,70]. We do not cover these approaches here.

F. Phononic Dissipation

Phononic confinement, propagation losses, and lifetimes are limited by various imperfections such as geometric disorder [35,52,60,71–73], thermo-elastic and Akhiezer damping [26,74,75], two-level systems [76–78], and clamping losses [34,79,80]. Losses in 2D-confined waveguides are typically quantified by a propagation length $L_m = \alpha_m^{-1}$ with α_m the propagation loss. In 3D-confined cavities, one usually quotes linewidths γ or quality factors $Q_m = \omega_m/\gamma$. A cavity's internal loss rate can be computed from the decay length L_m through $\gamma = v_m \alpha_m$ in high-finesse cavities with negligible bending losses [81] with v_m the mechanical group velocity. Mechanical propagation lengths in bulk crystalline silicon are limited to $L_m \approx 1$ cm at room temperature and at a frequency of $\omega_m/(2\pi) = 1$ GHz by thermo-elastic and Akhiezer damping. Equivalently, taking $v_m \approx 5000$ m/s, one can expect material-limited minimum linewidths of $\gamma/2\pi \approx 0.1$ MHz and maximum quality factors of $Q_m \approx 10^4$ [26,74] at $\omega_m/(2\pi) = 1$ GHz. Generally, crystalline materials have better intrinsic loss limits than polycrystalline and amorphous materials, while insulators have lower loss than semiconductors and metals [26].

These limits deteriorate rapidly at higher frequencies, typically scaling as $L_m \propto \omega_m^{-2}$ and $Q_m \propto \omega_m^{-1}$ [26,74,78] or worse. This makes the $f_m \cdot Q_m$ product a natural figure of merit for mechanical systems. For gigahertz-frequency resonators at room temperature, the highest demonstrated values of $f_m \cdot Q_m$ are on the order of 10^{13} in several materials [82]. Intriguingly, the maximum length of time that a quantum state can persist inside a mechanical resonator with quality factor Q_m at temperature T is given by $t_{\text{decoherence}} = \frac{\hbar Q_m}{kT}$, and so requiring that the information survive for more than a mechanical cycle is equivalent to the condition $t_{\text{decoherence}} > \omega_m^{-1}$, or $f_m \cdot Q_m > 6 \times 10^{12}$ Hz at room temperature [33]. This is usually seen as a necessary condition for optomechanics in the quantum regime, although pulsed measurements can relax this in some situations [83,84].

Recently, new loss-mitigation mechanisms called "dissipation dilution," "strain engineering," and "soft clamping" have been invented for megahertz mechanical resonators under tension that enable mechanical quality factors and $f_m \cdot Q_m$ products beyond 10^8 and 10^{15} Hz, respectively, under high vacuum but without refrigeration [85–87]. This unlocks exciting new possibilities for quantum-coherent operations at room temperature. These approaches are challenging to extend to stiff gigahertz mechanical modes as they require the elastic energy to be dominantly stored in the tension [88]. Finally, many material loss processes, with the possible exception of two-level systems [76,77,89], vanish rapidly at low temperatures (Section 4).

Despite impressive progress, the ultimate limits to phononic confinement are unknown and under active study (Section 4). Sidewall roughness and disorder pose a major roadblock in exploring these limits in the context of integrated phononics (Section 5.E).

3. PHOTON-PHONON INTERACTIONS

In this section, we describe the key mechanisms underpinning the coupling between photons and phonons. Photon-phonon interactions occur via two main mechanisms:

- Parametric coupling [Fig. 3(a)]: two photons and one phonon interact with each other in a three-wave mixing process as in Brillouin and Raman scattering and optomechanics, where the latter includes capacitive electromechanics.
- Direct coupling [Fig. 3(b)]: one photon and one phonon interact with each other directly as in piezoelectrics. This requires photons with a small frequency, as in the case of interactions between microwave photons and phonons.

The parametric three-wave mixing takes place via two routes:

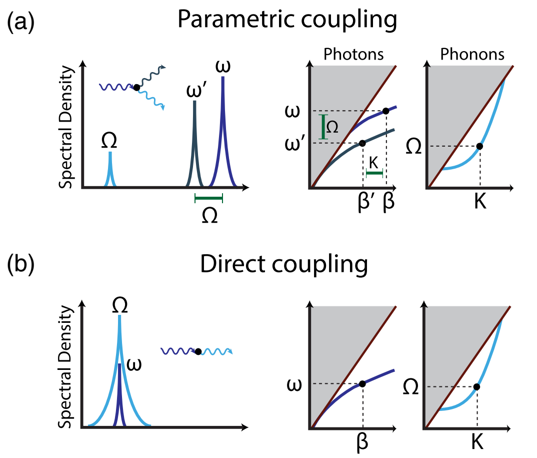

Fig. 3. Generating and detecting phonons. (a) Interactions between phonons and high-frequency photons occur through parametric three-wave mixing: two high-frequency photons couple to one phonon via third-order nonlinearities such as photoelasticity and the moving-boundary effect [96,97]. Interactions between low-frequency photons and a phonon can also occur through these mechanisms. Depending on which of the three waves is pumped, the interaction results in either down/upconversion ($\delta a \delta b + \text{h.c.}$) or state-swapping ($\delta a \delta b^\dagger + \text{h.c.}$) events. The frequency difference between the two high-frequency photons $\omega - \omega'$ must approximately equal the phononic frequency Ω for efficient parametric interactions to occur (left). In addition, in structures with translational symmetry, the wave vector difference between the two high-frequency photons $\beta - \beta'$ must also approximately equal the phononic wave vector K for efficient coupling (right). Here we depict only DFD; SFD proceeds analogously but with minus signs replaced by plus signs. (b) Direct conversion via second-order nonlinearities such as piezoelectricity is possible when the photonic energy is sufficiently low to match the phononic energy. Stronger mechanical waves can typically be generated by direct conversion than by indirect mixing of two optical waves (Section 5.B). A microwave photon can be converted into a phonon and subsequently into an optical photon by cascading two of these processes: either with one direct and one indirect process or with two indirect processes.

- Difference-frequency driving (DFD): two photons with frequencies ω and ω' drive the mechanical system through a beat note at frequency $\omega - \omega' = \Omega \approx \omega_m$ in the forces.
- Sum-frequency driving (SFD): two photons with frequencies ω and ω' drive the mechanical system through a beat note at frequency $\omega + \omega' = \Omega \approx \omega_m$ in the forces.

Three-wave DFD is the only possible mechanism when the photons and phonons have a large energy gap, as in interactions between phonons and optical photons. In contrast, microwave photons can interact with phonons through any of the three-wave and direct processes.

A. Interactions Between Phonons and Optical Photons

Parametric DFD in a cavity is generally described by an interaction Hamiltonian of the form (see Supplement 1):

$$\mathcal{H}_{\text{int}} = \hbar(\partial_x \omega_o) a^\dagger a x, \tag{1}$$

with $\partial_x \omega_o$ the sensitivity of the optical cavity frequency ω_o to mechanical motion x and a the photonic annihilation operator. The terminology "parametric" refers to the parameter ω_o, essentially the photonic energy, being modulated by the mechanical motion [90–93], whereas the term "three-wave mixing" points out that there are three operators in the Hamiltonian given by Eq. (1). This does not restrict the interaction to only three waves, as discussed further on. Describing the Hamiltonian $\mathcal{H}_{\text{int}}$ in this manner is a concise way of capturing all the consequences of the interaction between the electromagnetic field a and the mechanical motion x. The detailed dynamics can be studied via the Heisenberg equations of motion defined by $\dot{a} = -\frac{i}{\hbar}[a, \mathcal{H}_{\text{int}}]$ when making use of the harmonic oscillator commutator $[a, a^\dagger] = 1$ [33]. Since by definition $x = x_{zp}(\delta b + \delta b^\dagger)$ with x_{zp} the mechanical zero-point fluctuations and δb the phonon annihilation operator, this is equivalent to

$$\mathcal{H}_{\text{int}} = \hbar g_0 a^\dagger a (\delta b + \delta b^\dagger), \tag{2}$$

with

$$g_0 = (\partial_x \omega_o) x_{zp} \tag{3}$$

the zero-point optomechanical coupling rate, which quantifies the shift in the optical cavity frequency ω_o induced by the zero-point fluctuations x_{zp} of the mechanical oscillator. Here we neglect the static mechanical motion [33,94,95]. Achieving large g_0 thus generally requires small structures with large sensitivity $\partial_x \omega_o$ and zero-point motion $x_{zp} = (\hbar/(2\omega_m m_{\text{eff}}))^{1/2}$, where m_{eff} is the effective mass of the mechanical mode. This is brought about by ensuring a good overlap between the phononic field and the photonic forces acting on the mechanical system [34,96,97] and by focusing the photonic and phononic energy into a small volume to reduce m_{eff}. There are typically separate bulk and boundary contributions to the overlap integral. The bulk contribution is associated with photoelasticity, while the boundary contribution results from deformation of the interfaces between materials [96–99]. Achieving strong interactions requires careful engineering of a constructive interference between these contributions [34,96–98,100]. Optimized nanoscale silicon structures with mechanical modes at gigahertz frequencies typically have $x_{zp} \approx 1$ fm and $g_0/(2\pi) \approx 1$ MHz (Section 4). The zero-point fluctuation amplitude increases with lower frequency, leading to an increase in g_0: megahertz-frequency mechanical systems with $g_0/(2\pi) \approx 10$ MHz have been demonstrated [101].

The dynamics generated by the Hamiltonian of Eq. (2) can lead to a feedback loop. The beat note between two photons with slightly different frequencies ω and ω' generates a force that drives phonons at frequency $\omega - \omega' = \Omega$. Conversely, phonons modulate, at frequency Ω, the optical field, scattering photons into up- and downconverted sidebands. This feedback loop can amplify light or sound, lead to electromagnetically induced transparency, or cooling of mechanical modes. In principle, this interaction can cause nonlinear interactions at the few-photon or phonon limit if $g_0/\kappa > 1$ [102], though current solid-state systems are more than 2 orders of magnitude away from this regime (see Fig. 5 and Section 5.A).

Assuming $g_0/\kappa \ll 1$, valid in nearly all systems, we linearize the Hamiltonian of Eq. (2) by setting $a = \alpha + \delta a$ with α a classical, coherent pump amplitude, yielding

$$\mathcal{H}_{\text{int}} = \hbar g (\delta a + \delta a^\dagger)(\delta b + \delta b^\dagger), \tag{4}$$

with $g = g_0 \alpha$ the enhanced interaction rate—taking α real—and δa and δb the annihilation operators representing photonic and phononic signals, respectively. Often there are experimental conditions that suppress a subset of interactions present in

Hamiltonian (4). For instance, in sideband-resolved optomechanical cavities ($\omega_m > \kappa$), a blue-detuned pump α sets up an entangling interaction,

$$\mathcal{H}_{\mathrm{int}} = \hbar g(\delta a \delta b + \delta a^{\dagger} \delta b^{\dagger}) \tag{5}$$

that creates or annihilates photon-phonon pairs. Similarly, a red-detuned pump α sets up a beam-splitter interaction:

$$\mathcal{H}_{\mathrm{int}} = \hbar g(\delta a \delta b^{\dagger} + \delta a^{\dagger} \delta b) \tag{6}$$

that converts photons into phonons or vice versa. This beam-splitter Hamiltonian can also be realized by pumping the phononic instead of the photonic mode. In that case, α represents the phononic pump amplitude, whereas both δa and δb are then photonic signals.

In multimode systems, such as in 3D-confined cavities with several modes or in 2D-confined continuum systems, the interaction Hamiltonian is a summation or integration over each of the possible interactions between the individual photonic and phononic modes. For instance, linearized photon-phonon interactions in a 2D-confined waveguide with continuous translational symmetry are described by [103–105]:

$$\mathcal{H}_{\mathrm{int}} = \frac{\hbar}{\sqrt{2\pi}} \iint \mathrm{d}\beta \mathrm{d}K (g_{\beta+K} a_{\beta} b_K + g_{\beta-K} a_{\beta} b_K^{\dagger} + \mathrm{h.c.}). \tag{7}$$

In this case, the three-wave mixing interaction rate $g_{\beta+K} = g_{0|\beta+K} \alpha^{\star}_{\beta+K}$ is proportional to the amplitude $\alpha_{\beta+K}$ of the mode with wave vector $\beta + K$, which is usually considered to be pumped strongly. In contrast to the single-mode cavity described by Eq. (4), in the waveguide case, the symmetry between the two-mode-squeezing $\delta a \delta b$ and the beam-splitter $\delta a \delta b^{\dagger}$ terms is broken by momentum selection from the onset as generally $g_{\beta+K} \neq g_{\beta-K}$. The Hamiltonian of Eq. (7) assumes an infinitely long waveguide where phase-matching is strictly enforced. In contrast, a finite-length waveguide allows for interactions between a wider set of modes, although it suppresses those with a large phase mismatch (see Supplement 1). In essence, shorter waveguides permit larger violations of momentum conservation. The momentum selectivity enables nonreciprocal transport of both photons [106–109] and phonons [45,110]—in a continuum version of interference-based synthetic magnetism schemes using discrete optomechanical elements [59,111]. It also allows for sideband resolution even when the optical linewidth far exceeds the mechanical frequency [112].

Cavities can be realized by coiling up or terminating a 2D-confined waveguide with mirrors. Then the cavity's optomechanical coupling rate g_0 is connected to the waveguide's coupling rate $g_{0|\beta+K}$ by

$$g_0 = \frac{g_{0|\beta+K}}{\sqrt{L}}, \tag{8}$$

with L the roundtrip length of the cavity (see Supplement 1). The parameters $g_{0|\beta+K}$ and g_0 are directly related to the so-called Brillouin gain coefficient $\mathcal{G}_B$ that is often used to quantify photon-phonon interactions in waveguides [34,36,113]. In particular [81],

$$\mathcal{G}_B = \frac{4 g_{0|\beta+K}^2}{v_p v_s (\hbar\omega)\gamma}, \tag{9}$$

with v_p and v_s the group velocities of the interacting photons, $\hbar\omega$ the photon energy, and γ the phononic decay rate. Equations (8) and (9) enable comparison of the photon-phonon interaction strengths of waveguides and cavities. Since this gain coefficient depends on the mechanical quality factor Q_m via $\gamma = \omega_m / Q_m$, it is occasionally worth comparing waveguides in terms of the ratio $\mathcal{G}_B / Q_m$. The $g_0/(2\pi) \approx 1$ MHz measured in silicon optomechanical crystals [114] is via Eq. (9), in correspondence with the $\mathcal{G}_B / Q_m \approx 10\ \mathrm{W}^{-1}\ \mathrm{m}^{-1}$ measured in silicon nanowires at slightly higher frequencies [34,35]. Both g_0 and $\mathcal{G}_B / Q_m$ have an important dependence on mechanical frequency ω_m: lower-frequency structures are generally more flexible and thus generate larger interaction rates.

The Hamiltonians given in Eqs. (5), (6), and (7) describe a wide variety of effects. The detailed consequences of the three-wave mixing depend on the damping, intensity, dispersion, and momentum of the interacting fields. Next, we describe some of the potential dynamics. We quantify the dissipation experienced by the photons and phonons with decay rates κ and γ, respectively. The following regimes appear:

- Weak coupling: $g \ll \kappa + \gamma$. The phonons and photons can be seen as independent entities that interact weakly. A common figure of merit for the interaction is the cooperativity $\mathcal{C} = 4g^2/(\kappa\gamma)$, which quantifies the strength of the feedback loop discussed above. In particular, for $\mathcal{C} \gg 1$, the optomechanical back action dominates the dynamics. The pair-generation Hamiltonian (5) generates amplification, whereas the beam-splitter interaction (6) generates cooling and loss. Whether the phonons or the photons dominantly experience this amplification and loss depends on the ratio κ/γ of their decay rates. The linewidth of the phonons is effectively $(1 \mp \mathcal{C})\gamma$ when $\kappa \ll \gamma$, where the minus-sign in $\mp$ holds for the amplification case (Hamiltonian 5). In contrast, the linewidth of the photons is effectively $(1 \mp \mathcal{C})\kappa$ when $\gamma \ll \kappa$. A lasing threshold is reached for the phonons or the photons when $\mathcal{C} = 1$. In waveguide systems described by Eq. (7), $\mathcal{C} = 1$ is equivalent to the transparency point $\mathcal{G}_B P_p / \alpha = 1$, with P_p the pump power and α the waveguide propagation loss per meter. In fact, interactions between photons and phonons in a waveguide can also be captured in terms of a cooperativity that is identical to $\mathcal{C}$ under only weakly restrictive conditions [81].
- Strong coupling: $g \gg \kappa + \gamma$. The phonons and photons interact so strongly that they can no longer be considered independent entities. Instead, they form a photon-phonon polariton with an effective decay rate $(\kappa + \gamma)/2$. The beam-splitter interaction (6) sets up Rabi oscillations between photons and phonons with a period of $2\pi/g$ [33,115,116]. This is a necessary requirement for broadband intracavity state swapping, but is not strictly required for narrowband itinerant state conversion [117,118]. Strong coupling has been demonstrated in several systems [115,116, 119–121], but not yet in the single-photon regime (Section 5.A).

Neglecting dynamics and when the detuning from the mechanical resonance is large ($\Delta\Omega \gg \gamma$), the phonon ladder operator is $\delta b = (g_0/\Delta\Omega) a^{\dagger} a$ such that Hamiltonian (2) generates an effective dispersive Kerr nonlinearity described by

$$\mathcal{H}_{\mathrm{Kerr}} = \hbar \frac{g_0^2}{\Delta\Omega} a^{\dagger} a a^{\dagger} a. \tag{10}$$

This effective Kerr nonlinearity [122–126] is often much stronger than the intrinsic material nonlinearities. Thus, a single optomechanical system can mediate efficient and tunable interactions between up to four photons in a four-wave mixing process that annihilates and creates two photons. The mechanics enhances the intrinsic optical material nonlinearities for applications such as wavelength conversion [34,127,128]. Generally, such enhancements come at the cost of reduced bandwidth compared to intrinsic material nonlinearities. However, multimode effects can enable bandwidths far exceeding the intrinsic mechanical linewidth. For instance, a 2D-confined structure has a near-continuum set of mechanical modes. In a properly engineered structure, each of these modes might provide strong photon-phonon interactions.

Additional dynamical effects exist in the multimode case. For instance, in a waveguide described by Eq. (7), there is a spatial variation of the photonic and phononic fields that is absent in the optomechanical systems described by Eq. (4). This includes:

- The steady-state spatial Brillouin amplification of an optical sideband. This has been the topic of recent research in chip-scale photonic platforms. One can show that an optical Stokes sideband experiences a modified propagation loss $(1 - \mathcal{C})\alpha$, with $\mathcal{C} = \mathcal{G}_B P_p/\alpha$ the waveguide's cooperativity [81]. This Brillouin gain or loss is accompanied by slow or fast light [129,130]. Here we assumed an optical decay length exceeding the mechanical decay length, which is valid in nearly all systems. In the reverse case, the mechanical wave experiences a modified propagation loss $(1 - \mathcal{C})\alpha_m$, and there is slow and fast sound [81,131,132].
- Traveling photonic pulses can be converted into traveling phononic pulses in a bandwidth surpassing the mechanical linewidth. This is often called Brillouin light storage [133–136]. The traveling optical pump and signal pulses may counterpropagate or occupy different optical modes.

Several of these and other multimode effects have received little attention so far. This may change with the advent of new nanoscale systems realizing multimode and continuum Hamiltonians such as given in Eq. (7) with strong coupling rates [34,36,103,104,137].

B. Interactions Between Phonons and Microwave Photons

The above Section 3.A on parametric three-wave DFD also applies to interactions between phonons and microwave photons. However, microwave photons may interact with phonons via two additional routes: (1) three-wave SFD and (2) direct coupling. In three-wave SFD, two microwave photons with a frequency below the phonon frequency ω_m excite mechanical motion at the sum-frequency $\omega + \omega' = \Omega \approx \omega_m$ [4]. Such interactions can be realized in capacitive electromechanics, where the capacitance of an electrical circuit depends on mechanical motion. In particular, the capacitive coupling sets up an interaction,

$$\mathcal{H}_{\text{int}} = -\frac{(\partial_x C)V^2 x}{2}, \tag{11}$$

with $\partial_x C$ the sensitivity of the capacitance $C(x)$ to the mechanical motion x and V the voltage across the capacitor. In terms of ladder operators, we have $V = V_{zp}(a + a^\dagger)$ and $x = x_{zp}(\delta b + \delta b^\dagger)$ such that

$$\mathcal{H}_{\text{int}} = \hbar g_0\left(a^\dagger a + \frac{aa + a^\dagger a^\dagger}{2} + \frac{1}{2}\right)(\delta b + \delta b^\dagger). \tag{12}$$

Here the zero-point voltage is $V_{zp} = ((\hbar\omega_\mu)/(2C))^{1/2}$, with ω_μ the microwave frequency and C the total capacitance. This interaction contains three-wave DFD (Hamiltonian 2) as a subset via the $a^\dagger a$ term with an interaction rate g_0 given by

$$\hbar g_0 = -(\partial_x C)V_{zp}^2 x_{zp}. \tag{13}$$

In addition to three-wave DFD, it also contains three-wave SFD via the aa and $a^\dagger a^\dagger$ terms. These little-explored terms enable electromechanical interactions beyond the canonical three-wave DFD optomechanical and Brillouin interactions. Similar reasonings can be developed for inductively coupled mechanical resonators [138].

Further, by applying a strong bias voltage V_b, the capacitive interaction gets linearized: using $V = V_b + \delta V$ and keeping only the $2V_b\delta V$ term in V^2 yields

$$\mathcal{H}_{\text{int}} = -(\partial_x C)V_b \delta V x. \tag{14}$$

With $\delta V = V_{zp}(\delta a + \delta a^\dagger)$, this generates an interaction,

$$\mathcal{H}_{\text{int}} = \hbar g(\delta a + \delta a^\dagger)(\delta b + \delta b^\dagger), \tag{15}$$

which is identical to the linearized optomechanics Hamiltonian in expression (4) with an interaction rate set by

$$\hbar g = -(\partial_x C)V_b V_{zp} x_{zp} \tag{16}$$

that is enhanced with respect to g_0 by $g = g_0\alpha$ and $\alpha = V_b/V_{zp}$ the enhancement factor. The linearized Hamiltonian (15) realizes a tunable, effective piezoelectric interaction that can directly convert microwave photons into phonons and vice versa. Piezoelectric structures are described by Eq. (15) as well with an intrinsically fixed bias V_b determined by material properties.

The electromechanical coupling rate can be written as

$$g_0 = -\frac{\partial_x C}{2C}\omega_\mu x_{zp}, \tag{17}$$

or, alternatively, as $g_0 = (\partial_x \omega_\mu)x_{zp}$—precisely as in Section 3.A but with the optical frequency ω_o replaced by the microwave frequency ω_μ with $\omega_\mu = 1/\sqrt{L_{in}C}$ and L_{in} the circuit's inductance. Typically the capacitance $C = C_m(x) + C_p$ consists of a part that responds to mechanical motion $C_m(x)$ and a part C_p that is fixed and usually considered parasitic. This leads to

$$g_0 = -\frac{\partial_x C_m}{2C_m}\eta_p \omega_\mu x_{zp}, \tag{18}$$

with $\eta_p = C_m/C$ the participation ratio that measures the fraction of the capacitance responding to mechanical motion. For the canonical parallel-plate capacitor with electrode separation s, we have $\partial_x C_m = C_m/s$ such that $g_0 = -\eta_p x_{zp}\omega_\mu/(2s)$. This often drives research towards small structures with large zero-point motion x_{zp} and small electrode separation s. Contrary to the optical case, however, increasing the participation ratio η_p motivates increasing the size and thus the motional capacitance C_m of the structures until $\eta_p \approx 1$.

Finally, 3D-confined gigahertz mechanical modes have small mode volumes and motional capacitances C_m. They are difficult to match to common microwave circuits. This can be addressed by developing circuits with a small parasitic capacitance C_p and a large inductance L_{in} [119,139–142]. In gigahertz-range microwave circuits with unity participation and electrode separations on the order of $s \approx 100$ nm, we have $g_0/(2\pi) \approx -10$ Hz, about a factor $\omega_o/\omega_\mu \approx 10^5$ smaller than the optomechanical $g_0/(2\pi) \approx 1$ MHz (Section 3.A). Despite the much smaller g_0, it is still possible to achieve large cooperativity $\mathcal{C} = 4g^2/(\kappa\gamma)$ in electromechanics, as the typical microwave linewidths are much smaller and the enhancement factors α can be larger than in the optical case [139,141,142].

4. STATE OF THE ART

Here we give a concise overview of the current state of the art in opto- and electromechanical systems by summarizing the parameters obtained in about 50 opto- and electromechanical cavities and waveguides. The figures are not exhaustive. They are meant to give a feel for the variety of systems in the field. First, we plot the mechanical quality factors as a function of mechanical frequency (Fig. 4), including room temperature (red) and cold (blue) systems. As discussed in Section 2.F, cold systems usually reach much higher quality factors. The current record is held by a 5 GHz silicon optomechanical crystal with $Q_m > 10^{10}$, yielding a lifetime longer than a second [143] at millikelvin temperatures. Measuring these quality factors requires careful optically pulsed readout techniques, as the intrinsic dissipation of continuous-wave optical photons easily heats up the mechanics, thus destroying its coherence [144]. Comparably high quality factors are measured electrically in quartz and sapphire at lower frequencies [145,148]. It is an open question whether these extreme lifetimes have reached intrinsic material limits. The long lifetimes make mechanical systems attractive for delay lines and qubit storage [150] (Section 5). Figure 4 displays a rather weak link between mechanical frequency and quality factor. It also shows that 2D-confined systems have relatively low mechanical coherence so far, likely related to inhomogeneous effects [71].

Next, we look at the coupling strengths in these systems (Fig. 5). As discussed in Section 3, a few different figures of merit are commonly used, depending on the type of system. We believe the dimensionless ratios g_0/κ and the cooperativity $\mathcal{C}$ are two of the most powerful figures of merit (Section 5). The ratio g_0/κ determines the single-photon nonlinearity, the energy-per-bit in optical modulators, as well as the energy-per-qubit in microwave-to-optical photon converters. The cooperativity $\mathcal{C}$ must be unity for efficient state conversion as well as for phonon and photon lasing. In the context of waveguides, it measures the maximum Brillouin gain as $\mathcal{C} = \mathcal{G}_B P_p/\alpha$ [81].

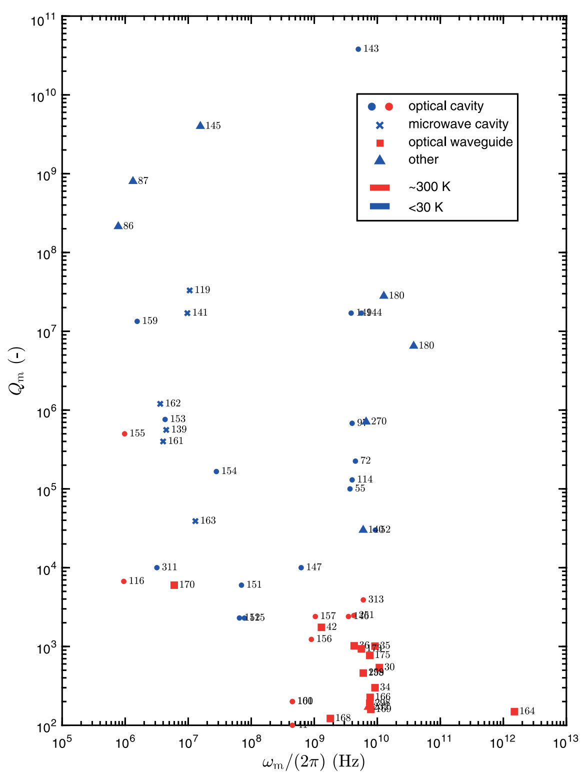

Fig. 4. Mechanical quality factors. The systems include opto- and electromechanical cavities and waveguides at room temperature (red), at a few kelvin (blue) and at millikelvin temperatures (blue). The highest quality factors are demonstrated in millikelvin cavities. The data points correspond to Refs. [30,34–36,41,42,52,55,72,86,87,97,101,114–116, 119,139–141,143–147,149,151–164,166,168–170,173,175,180,232, 251,270,298,299,311,313].

Thus we compute g_0/κ for about 50 opto- and electromechanical cavities and waveguides [Fig. 5(a)]. We convert the waveguide Brillouin coefficients $\mathcal{G}_B$ to g_0 via expressions (8) and (9) by estimating the minimum roundtrip length L a cavity made from the waveguide would have. In addition, we convert the waveguide propagation loss α to the intrinsic loss rate $\kappa_{in} = \alpha v_g$ with v_g the group velocity. This brings a diverse set of systems together in a single figure. No systems exceed $g_0/\kappa \approx 0.01$, with the highest values obtained in silicon optomechanical crystals [55,114], Brillouin-active waveguides [34,35,158], and Raman cavities [164]. There is no strong relation between g_0/κ and $\mathcal{C}$: systems with low interactions rates g_0 often have low decay rates κ and γ as well, since they do not have quite as stringent fabrication requirements on the surface quality.

The absolute zero-point coupling rates g_0 illustrate the power of moving to the nanoscale. We plot them as a function of the maximum quantum cooperativity $\mathcal{C}_q = \mathcal{C}/\bar{n}_{th}$ with $\bar{n}_{th}$ the thermal phonon occupation [Fig. 5(b)]. When $\mathcal{C}_q > 1$, the state transfer between photons and phonons takes place more rapidly than the mechanical thermal decoherence [33]. This is a requirement for hybrid quantum systems such as efficient microwave-to-optical photon converters (Section 5). There are several chip-scale electro- and optomechanical systems with $\mathcal{C}_q > 1$, with promising values demonstrated in silicon photonic crystals. An important impediment to large quantum cooperativities in optomechanics is the heating of the mechanics caused by optical absorption [144].

Further, we give an overview of the Brillouin coefficients $\mathcal{G}_B$ found in 2D-confined waveguides [Fig. 5(c)]. The current record $\mathcal{G}_B = 10^4\ \mathrm{W}^{-1}\ \mathrm{m}^{-1}$ in the gigahertz range was measured in a suspended series of silicon nanowires [35]. However, larger Brillouin amplification was obtained with silicon and chalcogenide rib waveguides, which have disproportionately lower optical propagation losses α and can handle larger optical pump powers P_p [158,165]. We stress that the maximum Brillouin gain is identical to the cooperativity [81]. They are both limited by the maximum power and electromagnetic energy density the system in question can withstand. At room temperature in silicon, the upper limit is usually set by two-photon and free-carrier absorption [34,36,99]. Moving beyond the two-photon bandgap of 2200 nm in silicon or switching to materials such as silicon nitride, lithium niobate, or chalcogenides can drastically improve the power handling [99,166,167,171,172]. In cold systems, it is instead set by the cooling power of the refrigerator and the heating of the mechanical system [144]. Another challenge for 2D-confined waveguides is the inhomogeneous broadening of the mechanical resonance. This arises from atomic-scale fluctuations in the waveguide geometry along its length, effectively smearing out the mechanical response [34–36,71]. In 2D-confined systems consisting of a series mechanically active sections [34,36], one must ensure that each section is sufficiently long to let the mechanical mode build up [174].

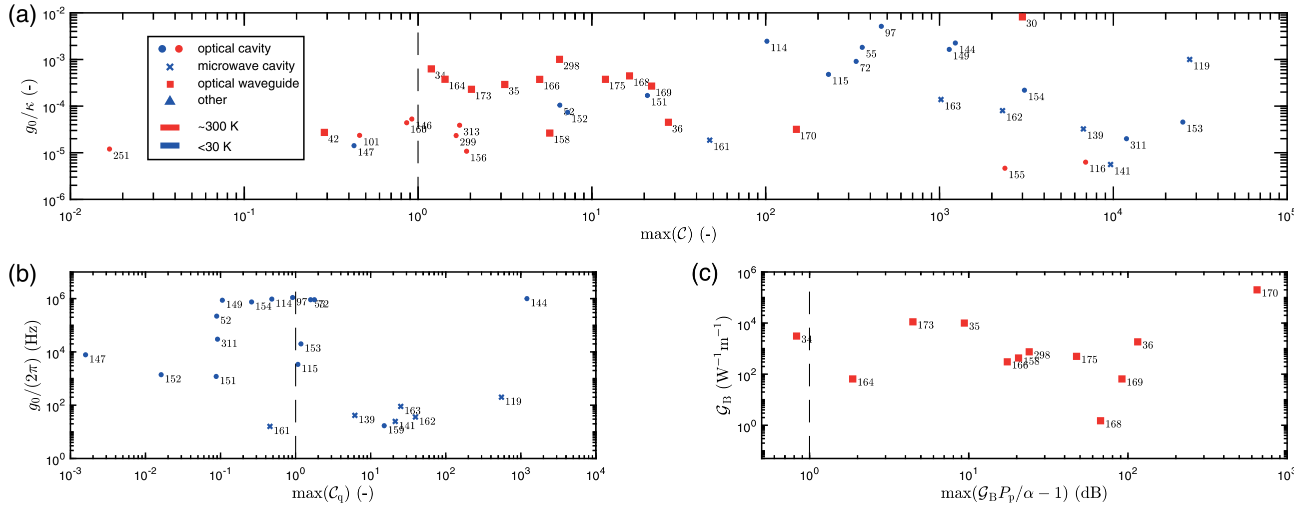

Fig. 5. Interaction rates in 3D-confined cavities and 2D-confined waveguides. (a) Dimensionless nonlinearity g_0/κ versus the maximum cooperativity $\mathcal{C}$. The largest interaction rates are achieved in nanoscale cavities and waveguides. Cooperativities are typically highest in cold systems (blue) and can be as high in less tightly confined systems, since they often have lower photonic and phononic decay rates than the smallest systems. Cavities so far achieve higher cooperativities than waveguides. This may change if the 2D-confined waveguide systems can be studied at low temperatures and if they can overcome inhomogeneous broadening. (b) Zero-point coupling rate g_0 versus the maximum quantum cooperativity $\mathcal{C}_q = \mathcal{C}/\bar{n}_{\text{th}}$ with $\bar{n}_{\text{th}}$ the thermal phonon occupation for a selection of cold 3D-confined systems. It is significantly harder to reach $\mathcal{C}_q > 1$ than $\mathcal{C} > 1$. In particular, optical absorption easily heats up mechanical systems—effectively increasing $\bar{n}_{\text{th}}$ [144]. (c) Brillouin gain coefficient $\mathcal{G}_B$ versus maximum net Brillouin gain $(\mathcal{G}_B P_p/\alpha - 1)$ for a selection of 2D-confined waveguides. Up to extrinsic cavity losses, $\mathcal{C} - 1 = (\mathcal{G}_B P_p/\alpha - 1)$. Achieving this maximum Brillouin gain requires the waveguide to have a length $L = 1/\alpha$, with α the optical propagation loss per meter. However, this is challenging as longer waveguides can—but do not always—suffer from inhomogeneous broadening of the mechanical resonance due to atomic-scale disorder in the waveguide geometry. Inhomogeneous effects are typically weaker in less confined systems. The data points correspond to Refs. [30,34–36,41,42,52,55,72,86,87,97,101,114–116,119,139–141,143–147,149,151–164,166,168–170,173,175,180,232,251,270,298,299,311,313]. There was no requirement for sideband resolution in these figures.

Finally, compared to gigahertz systems, flexible megahertz mechanical systems give much higher efficiencies of $\mathcal{G}_B \approx 10^6$ W^{-1} m^{-1} as measured in dual-nanoweb [176] fibers and of $\mathcal{G}_B \approx 10^9$ W^{-1} m^{-1}, as predicted in silicon double-slot waveguides [112]. In contrast to photonics, phononic systems have operating frequencies varying over many orders of magnitude: from kilohertz to gigahertz with acoustic phonons, and even terahertz with optical phonons. This is accompanied by great diversity in the mechanical structures. The choice of mechanical operating frequency can be influenced by many factors, including but not limited to the ability to passively freeze out thermal motion [177], to achieve spectral sideband resolution [178], large $f_m \cdot Q_m$ products [85,179], large zero-point motion x_{zp} [101,181,182], fast response [123], or better sensitivity [183]. The balance between the various trade-offs must be found case by case. Tightly confined gigahertz modes have attractive properties for low-energy communications, as discussed further on.

5. PERSPECTIVES

A. Single-Photon Nonlinear Optics

The three-wave mixing interactions discussed in Section 3 in principle enable single-photon nonlinear optics in opto- and electromechanical systems [102,184,185]. For instance, in the photon blockade effect, a single incoming photon excites the motion of a mechanical system in a cavity, which then shifts the cavity resonance and thus blocks the entrance of another photon. Realizing such quantum nonlinearities sets stringent requirements on the interaction strengths and decay rates.

For instance, in an optomechanical cavity, the force exerted by a single photon is $\langle F\rangle = -\langle \partial_x \mathcal{H}_{\text{int}}\rangle = -\hbar(g_0/x_{zp})\langle a^\dagger a\rangle = -\hbar(g_0/x_{zp})$. To greatly affect the optical response seen by another photon impinging on the cavity, this force must drive a mechanical displacement that shifts the optical resonance by about a linewidth κ or $x_\pi = \kappa/(\partial_x \omega_o) = (\kappa/g_0)x_{zp}$. In other words, we require $F/(m_{\text{eff}}\omega_m^2) = x_\pi$, which leads to $\vartheta_{\text{cav}} \equiv 4g_0^2/(\kappa\omega_m) \approx \pi$, where ϑ_{cav} is the mechanically mediated cross-phase shift experienced by the other photon, assuming critical coupling to the cavity. This extremely challenging condition is relaxed when two photonic modes with a frequency difference $\Delta\omega$ roughly resonant with the mechanical frequency are used. In this case, the mechanical frequency can be replaced by the detuning from the mechanical resonance in the above expressions: $\omega_m \to 2\Delta\Omega$ with the detuning $\Delta\Omega = \Delta\omega - \omega_m$. This enhances the shift per photon so that quantum nonlinearities are realized at [185,186]

$$\vartheta_{\text{cav}} = \frac{2g_0^2}{\kappa\Delta\Omega} \approx \pi, \tag{19}$$

with $\Delta\Omega \ll \omega_m$. The photon blockade effect also requires sideband resolution ($\Delta\Omega > \kappa$) so

$$\frac{g_0}{\kappa} > 1 \tag{20}$$

is generally a necessary condition for single-photon nonlinear optics with opto- and electromechanical cavities [33,187]. In the case of 2D-confined waveguides, it can similarly be shown [137] that a single photon drives a mechanically mediated cross-Kerr phase shift,

$$\vartheta_{\mathrm{wg}} = \frac{g^2_{0|\beta+K}}{v_{\mathrm{g}}\Delta\Omega}, \qquad (21)$$

on another photon with v_{g} the optical group velocity (see Supplement 1). The cross-Kerr phase shift ϑ_{wg} can be enhanced drastically by reducing the group velocity v_{g} via Brillouin slow light [130,137,188]. If sufficiently large, the phase shifts ϑ_{cav} and ϑ_{wg} can be used to realize controlled-phase gates between photonic qubits—an elementary building block for quantum information processors [137,189–191]. Using Eq. (8), we have

$$\vartheta_{\mathrm{cav}} = \frac{\mathcal{F}}{\pi}\vartheta_{\mathrm{wg}}, \qquad (22)$$

with $\mathcal{F} = 2\pi/(\kappa T_{\mathrm{rt}})$ the cavity finesse and T_{rt} the cavity round-trip time. Therefore, cavities generally yield larger single-photon cross-Kerr phase shifts than their corresponding optomechanical waveguides.

Currently state-of-the-art solid-state and sideband-resolved ($\omega_{\mathrm{m}} > \kappa$) opto- and electromechanical systems yield at best $g_0/\kappa \approx 0.01$ in any material (Fig. 5). Significant advances in g_0 may be made in, e.g., nanoscale-slotted structures [101,192,193], but it remains an open challenge to not only increase g_0 but also g_0/κ by a few orders of magnitude [194]. Beyond exploring novel structures, other potential approaches include effectively boosting g_0/κ by parametrically amplifying the mechanical motion [195], by employing delayed quantum feedback [196], or via collectively enhanced interactions in optomechanical arrays [197,198]. Although single-photon nonlinear optics may be out of reach for now, many-photon nonlinear optics can be enhanced very effectively with mechanics. Specifically, mechanics realizes Kerr nonlinearities orders of magnitude beyond those of typical intrinsic material effects. This is especially so for highly flexible, low-frequency mechanical systems [122,123,199,200], but has been shown in gigahertz silicon optomechanical cavities and waveguides as well [34,127].

B. Efficient Optical Modulation

Phonons provide a natural means for the spatiotemporal modulation of optical photons via electro- and optomechanical interactions. Hybrid circuits that marry photonic and phononic excitations give us access to novel opto-electromechanical systems. Two aspects of the physics make phononic circuits very attractive for the modulation of optical fields.

First, there is excellent spatial matching between light and sound. As touched upon above, the wavelengths of microwave phonons and telecom photons are both about a micron in technologically relevant materials such as silicon. The matching follows from the 4 to 5 orders of magnitude difference between the speed of sound and the speed of light. Momentum conservation, i.e., phase-matching, between phonons and optical photons (as discussed in Section 3) is key for nonreciprocal nonlinear processes and modulation schemes with traveling phonons [59,106,108,201].

Second, the optomechanical nonlinearity is strong and essentially lossless. Small deformations can induce major changes on the optical response of a system. For instance, in an optomechanical cavity [Eq. (1)], the mechanical motion required to encode a bit onto a light field has an amplitude of approximately $x_\pi = (\kappa/g_0)x_{\mathrm{zp}}$. Generating this motion requires energy, and this corresponds to an energy-per-bit $E_{\mathrm{bit}} = m_{\mathrm{eff}}\omega_{\mathrm{m}}^2 x_\pi^2/2$, which we rewrite as

$$E_{\mathrm{bit}} = \frac{\hbar\omega_{\mathrm{m}}}{4}\left(\frac{\kappa}{g_0}\right)^2. \qquad (23)$$

Thus the energy-per-bit also depends on the dimensionless quantity g_0/κ: a single phonon can switch a photon when this quantity reaches unity, in agreement with Section 5.A. For silicon optomechanical crystals with $g_0/\kappa \approx 10^{-3}$, this yields $E_{\mathrm{bit}} \approx 1\,\mathrm{aJ/bit}$: orders of magnitude more efficient than commonly deployed electro-optic technologies [11].

The similarity between the fundamental interactions in optomechanics [33] and electro-optics [202,203] allows one to compare the two types of modulation head-to-head. In particular, in an optical cavity made of an electro-optic material the voltage drop across the electrodes required to encode a bit is $V_\pi = \kappa/(\partial_V\omega_{\mathrm{o}}) = (\kappa/g_0)V_{\mathrm{zp}}$, with $g_0 = (\partial_V\omega_{\mathrm{o}})V_{\mathrm{zp}}$ the electro-optic interaction rate [202,203], which is defined analogously to the optomechanical interaction rate. It is the parameter appearing in the interaction Hamiltonian $\mathcal{H}_{\mathrm{int}} = \hbar g_0 a^\dagger a(b + b^\dagger)$, with $b + b^\dagger$ now proportional to the voltage across the capacitor of a microwave cavity [202,203]. The required V_π corresponds to an energy-per-bit $E_{\mathrm{bit}} = CV_\pi^2/2$, which again can be rewritten as expression (23). Electro-optic materials such as lithium niobate [204] may yield up to $g_0/(2\pi) \approx 10$ kHz, corresponding to an energy-per-bit $E_{\mathrm{bit}} \approx 10$ fJ/bit, keeping the optical linewidth κ constant—on the order of today's world records [11].

Although full system demonstrations using mechanics for electro-optic modulation are lacking, based on estimates like these we believe that mechanics will unlock highly efficient electro-optic systems. The expected much lower energy-per-bit implies that future electro-optomechanical modulators could achieve much higher bit rates at fixed power, or alternatively, much lower dissipated power at fixed bit rate than current direct electro-optic modulators. Although the mechanical linewidth does not enter expression (23), bandwidths of a single device are usually limited by the phononic quality factor or transit time across the device. Interestingly, the mechanical displacement corresponding to the estimated 1 aJ/bit is only $x_\pi \approx 10$ pm.

Here we highlighted the potential for optical modulation based on mechanical motion at gigahertz frequencies. However, similar arguments can be made for optical switching networks based on lower frequency mechanical structures. In particular, voltage-driven capacitive or piezoelectric optical phase-shifters exploiting mechanical motion do not draw static power and can generate large optical phase shifts in small devices [205–212]. These photonic micro-electromechanical systems (MEMS) are thus an attractive elementary building block in reconfigurable and densely integrated photonic networks used for high-dimensional classical [11, 213–216] and quantum [217–220] photonic information processors. They may meet the challenging power and space constraints involved in running a complex programmable network.

Demonstrating fully integrated acousto-optic systems requires that we properly confine, excite, and route phonons on a chip. Among the currently proposed and demonstrated systems are acousto-optic modulators [108], as well as optomechanical beam-steering systems [73,221]. Besides showing the power of sound to process light with minuscule amounts of energy, these phononic systems have features that are absent in competing approaches. For instance, gigahertz traveling mechanical waves with large momentum naturally enable nonreciprocal features in both modulators [108] and beam-steering systems [73].

This is essential for isolators and circulators based on indirect photonic transitions [107,222–227].

In order to realize these and other acousto-optic systems, it is crucial to efficiently excite mechanical excitations on the surface of a chip. In this context, electrical excitation is especially promising, as it allows for stronger mechanical waves than optical excitation. With optical excitation of mechanical waves, the flux of phonons is upper-bounded by the flux of optical photons injected into the structure. The ratio of photon to phonon energy limits the mechanical power to less than a microwatt, corresponding to 10–100 mW of optical power. Nevertheless, proof-of-concept demonstrations [107,109,228] have successfully generated nonreciprocity on a chip using optically generated phonons. In contrast, microwave photons have a factor 10^5 larger fluxes than optical photons for the same power. Therefore, microwave photons can drive milliwatt-level mechanical waves in nanoscale cavities and waveguides. Such mechanical waves can have displacements up to a nanometer and strains of a few percent—close to material yield strengths.

Electrical generation of gigahertz phonons in nanoscale structures has received little attention so far, especially in nonpiezoelectric materials such as silicon and silicon nitride. As discussed in Section 3.B, this can be realized either via capacitive or via piezoelectric electromechanics. Capacitive approaches work in any material [229–231] and have recently been demonstrated in a silicon photonic waveguide [232]. They require small capacitor gaps and large bias voltages to generate effects of magnitude comparable to piezoelectric approaches. More commonly, piezoelectrics such as gallium arsenide [58,233], lithium niobate, aluminum nitride [234,235], and lead-zirconate titanate can be used as the photonic platform, or be integrated with existing photonic platforms such as silicon and silicon nitride in order to combine the best of both worlds [73,236–239]. Such hybrid integration typically comes with challenging incompatibilities in material properties [240], especially when more than one material needs to be integrated on a single chip. Efficient electrically driven acoustic waves in photonic structures have the potential to enable isolation and circulation with an optical bandwidth beyond 1 THz—limited only by optical walk-off [106,227,241–244].

C. Hybrid Quantum Systems

Strain and displacement alter the properties of many different systems and therefore provide excellent opportunities for connecting dissimilar degrees of freedom. In addition, mechanical systems can possess very long coherence times and can be used to store quantum information. In the field of hybrid quantum systems, researchers find ways to couple different degrees of freedom over which quantum control is possible to scale up and extend the power of quantum systems. Realizing hybrid systems by combining mechanical elements with other excitations is a widely pursued research goal. Studies on both static tuning of quantum systems using nanomechanical forces [245–248] as well as on quantum dynamics mediated by mechanical resonances and waveguides [62,177,246,249,250] are being pursued.

Among the emerging hybrid quantum systems, microwave-to-optical photon converters utilizing mechanical degrees of freedom have attracted particular interest recently [249,251–255]. In particular, one of the leading platforms to realize scalable, error-corrected quantum processors [256,257] is superconducting microwave circuits in which qubits are realized using Josephson junctions [258,259] in a platform compatible with silicon photonics [260]. To suppress decoherence, these microwave circuits are operated at millikelvin temperatures inside dilution refrigerators. Heat generation must be restricted in these cold environments [261]. The most advanced prototypes currently consist of on the order of 50 qubits on which gates with at best 0.1% error rates can be applied [261,262]. Scaling up these systems to millions of qubits, as required for a fully error-corrected quantum computer, is a formidable unresolved challenge [257]. Also, the flow of microwave quantum information is hindered outside of the dilution refrigerators by the microwave thermal noise present at room temperature [263,264]. Optical photons travel for kilometers at room temperature along today's optical fiber networks. Thus quantum interfaces that convert microwave to optical photons with high efficiency and low noise should help address the scaling and communication barriers hindering microwave quantum processors. They may pave the way for distributed and modular quantum computing systems or a "quantum Internet" [265,266]. Besides, such interfaces would give optical systems access to the large nonlinearities generated by Josephson junctions, which enables a new approach for nonlinear optics.

The envisioned microwave-to-optical photon converters are in essence electro-optic modulators that operate on single photons and preserve entanglement [202]. They exploit the beam-splitter Hamiltonian discussed in Section 3 to swap quantum states from the microwave to the optical domain and vice versa. To realize a microwave-to-optical photon converter, one can start from a classical electro-optic modulator and modify it to protect quantum coherence. Several proposals aim to achieve this by coupling a superconducting microwave cavity to an optical cavity made of an electro-optic material. For instance, the beam-splitter Hamiltonian can be engineered by injecting a strong optical pump red-detuned from the cavity resonance in an electro-optic cavity. In order to suppress undesired Stokes scattering events, the frequency of the microwave cavity needs to exceed the optical cavity linewidth, i.e., sideband resolution is necessary. In this scenario, continuous-wave state conversion with high fidelity requires an electro-optic cooperativity $\mathcal{C}_{\mathrm{eo}}$ close to unity:

$$\mathcal{C}_{\mathrm{eo}} = \frac{4g_0^2|\alpha|^2}{\kappa\gamma_\mu} = 1, \tag{24}$$

with g_0 the electro-optic interaction rate as defined in the previous section, $|\alpha|^2$ the number of optical pump photons in the cavity, and γ_μ the microwave cavity linewidth. The quantum conversion is accompanied by an optical power dissipation $P_{\mathrm{diss}} = \hbar\omega_{\mathrm{o}}|\alpha|^2\kappa_{\mathrm{in}}$, with κ_{in} the intrinsic decay rate of the optical cavity. Operating the converter in a bandwidth of γ_μ and inserting condition (24), this leads to an energy-per-qubit of

$$E_{\mathrm{qbit}} = \frac{\hbar\omega_{\mathrm{o}}}{4}\left(\frac{\kappa\kappa_{\mathrm{in}}}{g_0^2}\right), \tag{25}$$

which is the quantum version of the energy-per-bit (23). This yields an interesting relation between the efficiency of classical and quantum modulators:

$$\frac{E_{\mathrm{qbit}}}{E_{\mathrm{bit}}} \approx \frac{\omega_{\mathrm{o}}}{\omega_{\mathrm{m}}}. \tag{26}$$

We stress that E_{qbit} is the optical dissipated energy in a quantum converter, whereas E_{bit} is the microwave or mechanical energy necessary to switch an optical field in a classical modulator [267]. The quantum electro-optic modulator dissipates roughly 5 orders of magnitude more energy per converted qubit, as it requires an optical pump field to drive the conversion process. Strategies developed to minimize E_{bit}, as pursued for decades by academic groups and the optical communications industry, also tend to minimize E_{qbit}. Recently, a coupling rate of $g_0/(2\pi) = 310$ Hz was demonstrated in an integrated aluminum nitride electro-optic resonator [268]. Switching to lithium niobate and harnessing improvements in the electro-optic modal overlap may increase this to $g_0/(2\pi) \approx 10$ kHz, corresponding to $E_{\mathrm{qbit}} \approx 1$ nJ/qbit. Electro-optic polymers [269] may yield higher interaction rates g_0 but bring along challenges in optical and microwave losses κ and γ_μ. Cooling powers of roughly 10 μW at the low-temperature stage of current dilution refrigerators [261] imply that conversion rates with common electro-optic materials will likely not exceed about 10 kqbits/s.

Considering that the g_0/κ demonstrated optomechanical devices are much larger than those found in electro-optic systems, and following a reasoning similar to that presented in Section 5.B for classical modulators, it is likely that microwave-to-optical photon converters based on mechanical elements as intermediaries will be able to achieve large efficiencies. It has been theoretically shown that electro-optomechanical cavities with dynamics described in Section 3 allow for efficient state transduction between microwave and optical fields when

$$\mathcal{C}_{\mathrm{em}} \approx \mathcal{C}_{\mathrm{om}} \gg 1, \tag{27}$$

with $\mathcal{C}_{\mathrm{em}}$ and $\mathcal{C}_{\mathrm{om}}$ the electro- and optomechanical cooperativities. Noiseless conversion additionally requires negligible thermal microwave and mechanical occupations [117,118,252]. Since the dominant dissipation still arises from the optical pump, the energy-per-qubit can still be expressed as in Eq. (25) for a electro-optomechanical cavity. Given the large nonlinearity g_0/κ enabled by nanoscale mechanical systems (Fig. 5), we expect conversion rates up to 100 Mqbits/s are feasible by operating multiple electro-optomechanical photon converters in parallel inside the refrigerator. State-of-the-art integrated electro- and optomechanical cavities have achieved $\mathcal{C}_{\mathrm{em}} > 1$ and $\mathcal{C}_{\mathrm{om}} > 1$ in separate systems (Fig. 5). It is an open challenge to achieve condition (27) in a single integrated electro-optomechanical device.

Finally, the long lifetimes and compact nature of mechanical systems also makes them attractive for the storage of classical and quantum information [140,150,183,250,270–275]. Mechanical memories are currently pursued both with purely electromechanical [140,177,270] and purely optomechanical [133,134] systems. Interfaces between mechanical systems and superconducting qubits may lead to the generation of nonclassical states of mesoscopic mechanical systems [33,271,276–281], probing the boundary between quantum and classical behavior.

D. Microwave Signal Processing

In particular, in the context of wireless communications, compact and cost-effective solutions for radio-frequency (RF) signal processing are rapidly gaining importance. Compared to purely electronic and MEMS-based approaches, RF processing in the photonics domain—microwave photonics—promises compactness and light weight, rapid tunability, and integration density [282–284]. Currently demonstrated optical solutions, however, still suffer from high RF-insertion loss and an unfavorable trade-off between achieving sufficiently narrow bandwidth, high rejection ratio, and linearity. Solutions mediated by phonons might overcome this limit, as they offer a narrow linewidth without suffering from the power limits experienced in high-quality optical cavities [165,285].

Given the high power requirements, 2D-confined waveguides lend themselves more naturally to many RF applications. As such, stimulated Brillouin scattering (SBS) has been extensively exploited. Original work focused on phonon-photon interactions in optical fibers, which allows for high SBS gain and high optical power but lacks compactness and integrability. Following the demonstration of SBS gain in integrated waveguide platforms [34,36,166], several groups now also demonstrated RF signal processing using integrated photonics chips. In the most straightforward approach, the RF signal is modulated on a sideband of an optical carrier which is then overlaid with the narrowband SBS loss spectrum generated by a strong pump [286,287]. Tuning the carrier frequency allows rapid and straightforward tuning of the notch filter over several gigahertz and a bandwidth below 130 MHz was demonstrated. The suppression was only 20 dB, however, limited by the SBS gain achievable in the waveguide platform used, in this case a chalcogenide waveguide. This issue is further exacerbated in more complementary metal–oxide–semiconductor (CMOS)-compatible platforms, where the SBS gain is typically limited to a few decibels. This can be overcome by using interferometric approaches, which enable over 45 dB suppression with only 1 dB of SBS gain [288,289].

While this approach outperforms existing photonic and nonphotonic approaches on almost all specifications (see Table 1 in [288]), a remaining issue is the high RF insertion loss of about 30 dB. Integration might be key in bringing the latter to a competitive level, as excessive fiber-to-chip losses and high modulator drive voltages associated with the discrete photonic devices currently being used are the main origin of the low system efficiency. Also, the photonic-phononic emit-receive scheme proposed in [227,290] results in a lower RF insertion loss. Although it gives up tunability, additional advantages of this approach are its engineerable filter response [290,291] and its cascadability [227]. Exploiting the phase response of the SBS resonance also phase control of RF signals has been demonstrated [285]. Phase control of RF signals via the phase response of the SBS resonance has also been demonstrated. Again, interferometric approaches allow one to amplify the intrinsic phase delay of the system, which is limited by the available SBS gain. In the examples above, the filter is driven by a single-frequency pump, resulting in a Lorentzian filter response. More complex filter responses can be obtained by combining multiple pumps [130]. However, this comes at the cost of the overall system response, since the total power handling capacity of the system is typically limited. As such, there is still a need for waveguide platforms that can handle large optical powers and at the same time provide high SBS gain.

Further, low-noise oscillators are also a key building block in RF systems. In [292], an SBS-based narrowband tunable filter is integrated in the fiber loop of a hybrid opto-electronic oscillator (OEO), allowing single-mode operation and wide frequency tunability. Also, oscillators fully relying on optomechanical interactions have been demonstrated. Two approaches, equivalent with the two dissipation hierarchies ($\gamma \gg \kappa$ and $\gamma \ll \kappa$) identified in Section 3, have been studied. In the first case, if the photon lifetime exceeds the phonon lifetime ($\gamma \gg \kappa$), optical line narrowing and eventually self-oscillation is obtained at the transparency condition $\mathcal{C} = 1$—resulting in substantial narrowing of the Stokes wave and thus a purified laser beam [293–295].

Cascading this process leads to higher-order Stokes waves with increasingly narrowed linewidths. Photomixing a pair of cascaded Brillouin lines gives an RF carrier with phase noise determined by the lowest-order Stokes wave. Using this approach in a very low-loss silica disk resonator, a phase noise suppression of 110 dBc at 100 kHz offset from a 21.7 GHz carrier was demonstrated [296]. In the alternate case, with the phonon lifetime exceeding the photon lifetime ($\gamma \ll \kappa$), the Stokes wave is a frequency-shifted copy of the pump wave apart from the phase noise added by the mechanical oscillator. At the transparency condition $\mathcal{C} = 1$, the phonon noise goes down, eventually reaching the mechanical Schawlow–Townes limit [297]. Several such "phonon lasers" have been demonstrated already, relying on very different integration platforms [298–302]. Further work is needed to determine if these devices can deliver the performance required to compete with existing microwave oscillators.

In the examples above, the mechanical mode is excited all-optically via a strong pump beam. Both in terms of efficiency and in terms of preventing the pump beam from propagating further through the optical circuit, this may be not the most appropriate method. Recently, several authors have demonstrated electrical actuation of optomechanical circuits [58,108,232,251,303–305]. While this provides a more direct way to drive the acousto-optic circuit, considerable efforts are still needed to improve the overall efficiency of these systems and to develop a platform where all relevant building blocks including, e.g., actuators and detectors, optomechanical oscillators, and acoustic delay lines can be co-integrated without loss in performance.

E. General Challenges

Each of the perspectives discussed above potentially benefits enormously from miniaturizing photonic and phononic systems in order to maximize interaction rates and pack more functionality into a constrained space. Current nanoscale electro- and optomechanical devices indeed demonstrate some of the highest interaction rates (Section 4). However, the fabrication of high-quality nanoscale systems requires exquisite process control. Even atomic-scale disorder in the geometric properties can hamper device performance, especially when extended structures or many elements are required [35,306,307]. This can be considered the curse of moving to the nanoscale. It manifests itself as photonic and phononic propagation loss [61,72], backscattering [61], intermodal scattering, as well as inhomogeneous broadening [71], dephasing [73], and resonance splitting [35,52].

To give a feel for the sensitivity of these systems, a 10 GHz mechanical breathing mode undergoes a frequency shift of about 10 MHz per added monolayer of silicon atoms [34]. Therefore, nanometer-level disorder is easily resolvable in current devices with room-temperature quality factors on the order of 10^3. Developing better process control and local tuning [308] methods is thus a major task for decades to come. In addition, shrinking systems to the nanoscale leads to large surface-to-volume ratios that imply generally ill-understood surface physics determines key device properties, even with heavily studied materials such as silicon [97,309,310]. This is a particular impediment for emerging material platforms such as thin-film aluminum nitride [311], lithium niobate [312], and diamond [313–315]. The flip side of these large sensitivities is that opto- and electromechanical systems may generate exquisite sensors of various perturbations. Among others, current sensor research takes aim at inertial and mass sensing [179,316–318], as well as local temperature [319] and geometry mapping [320–323].

Finally, tight confinement restricts the number of photons that can be loaded into the system. This influences not merely the maximum cooperativity, but also the thermal phonon occupation. A key target of high confinement systems is increasing the unitless nonlinearity g_0/κ and the cooperativity $\mathcal{C}$, enhancing the interaction rates faster than various parasitic effects. Continued investments in nanotechnology give hope for further progress on this front.

6. CONCLUSION

New hybrid electro- and optomechanical nanoscale systems have emerged in the last decade. These systems confine both photons and phonons in structures about one wavelength across to set up large interaction rates in a compact space. Similar to integrated photonics more than a decade ago, nanoscale *phononic* circuitry is in its infancy and severe challenges such as geometric disorder hinder its development. Still, we expect much to come in the years ahead. We believe mechanical systems are particularly interesting as low-energy electro-optic interfaces with potential use in coherent classical and quantum information processors and sensors. Phonons are a gateway for photons to a world with 5 orders of magnitude slower time scales. Linking the two excitations has the potential for major impact on our information infrastructure in ways we have yet to fully explore.

Funding. National Science Foundation (NSF) (ECCS-1509107, ECCS-1708734); David and Lucile Packard Foundation (David and Lucile Packard Fellowship); Horizon 2020 Framework Programme (H2020) (Marie Sklodowska-Curie grant agreement No. 665501); Fonds Wetenschappelijk Onderzoek (FWO) (Marie Sklodowska-Curie grant agreement No. 665501); Air Force Office of Scientific Research (AFOSR) (MURI); VOCATIO.

Acknowledgment. R. V. L. organized and wrote much of the paper along with A. S. N. The section on microwave signal processing was written by D. V. T. All authors read, discussed, and gave critical feedback on the paper. The authors are grateful to two anonymous referees for helpful feedback.

See Supplement 1 for supporting content.

REFERENCES

1. C. T.-C. Nguyen, "MEMS-based RF channel selection for true software-defined cognitive radio and low-power sensor communications," IEEE Commun. Mag. **51**, 110–119 (2013).
2. K. Hashimoto, *Surface Acoustic Wave Devices in Telecommunications* (Springer, 2000).
3. K. Hashimoto, *RF Bulk Acoustic Wave Filters for Communications* (Artech House, 2009), p. 267.
4. T. B. Jones and N. G. Nenadic, *Electromechanics and MEMS* (Cambridge University, 2013).
5. R. C. Ruby, P. Bradley, Y. Oshmyansky, A. Chien, and J. D. Larson, "Thin film bulk wave acoustic resonators (FBAR) for wireless applications," in *IEEE Ultrasonics Symposium Proceedings: An International Symposium*, 2001, pp. 813–821.
6. R. C. Ruby, "Review and comparison of bulk acoustic wave FBAR, SMR technology," in *IEEE Ultrasonics Symposium Proceedings* (IEEE, 2007), pp. 1029–1040.

7. M. Hara, J. Kuypers, T. Abe, and M. Esashi, “Surface micromachined AlN thin film 2 GHz resonator for CMOS integration,” Sens. Actuators A, Phys. **117**, 211–216 (2005).
8. H. Bhugra and G. Piazza, eds., *Piezoelectric MEMS Resonators, Microsystems and Nanosystems* (Springer International Publishing, 2017).
9. D. Van Thourhout and J. Roels, “Optomechanical device actuation through the optical gradient force,” Nat. Photonics **4**, 211–217 (2010).
10. B. E. Little and S. T. Chu, “Toward very large-scale integrated photonics,” Opt. Photon. News **11**(11), 24–28 (2000).
11. D. A. Miller, “Attojoule optoelectronics for low-energy information processing and communications,” J. Lightwave Technol. **35**, 346–396 (2017).
12. Z. Wang, A. Abbasi, U. Dave, A. De Groote, S. Kumari, B. Kunert, C. Merckling, M. Pantouvaki, Y. Shi, B. Tian, K. Van Gasse, J. Verbist, R. Wang, W. Xie, J. Zhang, Y. Zhu, J. Bauwelinck, X. Yin, Z. Hens, J. Van Campenhout, B. Kuyken, R. Baets, G. Morthier, D. Van Thourhout, and G. Roelkens, “Novel light source integration approaches for silicon photonics,” Laser Photon. Rev. **11**, 1700063 (2017).
13. C. Sun, M. T. Wade, Y. Lee, J. S. Orcutt, L. Alloatti, M. S. Georgas, A. S. Waterman, J. M. Shainline, R. R. Avizienis, S. Lin, B. R. Moss, R. Kumar, F. Pavanello, A. H. Atabaki, H. M. Cook, A. J. Ou, J. C. Leu, Y.-H. Chen, K. Asanović, R. J. Ram, M. A. Popović, and V. M. Stojanović, “Single-chip microprocessor that communicates directly using light,” Nature **528**, 534–538 (2015).
14. A. Rahim, E. Ryckeboer, A. Subramanian, S. Clemmen, B. Kuyken, A. Dhakal, A. Raza, A. Hermans, M. Muneeb, S. Dhoore, Y. Li, U. Dave, P. Bienstman, N. LeThomas, G. Roelkens, D. Van Thourhout, X. Rottenberg, P. Helin, S. Severi, and R. Baets, “Expanding the silicon photonics portfolio with silicon nitride photonic integrated circuits,” J. Lightwave Technol. **35**, 639–649 (2017).
15. A. H. Atabaki, S. Moazeni, F. Pavanello, H. Gevorgyan, J. Notaros, L. Alloatti, M. T. Wade, C. Sun, S. A. Kruger, H. Meng, K. A. Qubaisi, I. Wang, B. Zhang, A. Khilo, C. V. Baiocco, M. A. Popović, V. M. Stojanović, and R. J. Ram, “Integrating photonics with silicon nanoelectronics for the next generation of systems on a chip,” Nature **556**, 349–354 (2018).
16. R. Soref, “The past, present, and future of silicon photonics,” IEEE J. Sel. Top. Quantum Electron. **12**, 1678–1687 (2006).
17. E. Garmire, “Stimulated Brillouin review: invented 50 years ago and applied today,” Int. J. Opt. **2018**, 1–17 (2018).
18. A. Rahim, T. Spuesens, R. Baets, and W. Bogaerts, “Open-access silicon photonics: current status and emerging initiatives,” Proc. IEEE **106**, 2313–2330 (2018).
19. A. Boes, B. Corcoran, L. Chang, J. Bowers, and A. Mitchell, “Status and potential of lithium niobate on insulator (LNOI) for photonic integrated circuits,” Laser Photon. Rev. **12**, 1700256 (2018).
20. V. M. N. Passaro, F. Magno, and F. De Leonardis, “Optimization of Bragg reflectors in AlGaAs/GaAs VCSELs,” Laser Phys. Lett. **2**, 239–246 (2005).
21. M. Goryachev, D. L. Creedon, E. N. Ivanov, S. Galliou, R. Bourquin, and M. E. Tobar, “Extremely low-loss acoustic phonons in a quartz bulk acoustic wave resonator at millikelvin temperature,” Appl. Phys. Lett. **100**, 243504 (2012).
22. B. J. Eggleton, B. Luther-Davies, and K. Richardson, “Chalcogenide photonics,” Nat. Photonics **5**, 141–148 (2011).
23. S. Volz, J. Ordonez-Miranda, A. Shchepetov, M. Prunnila, J. Ahopelto, T. Pezeril, G. Vaudel, V. Gusev, P. Ruello, E. M. Weig, M. Schubert, M. Hettich, M. Grossman, T. Dekorsy, F. Alzina, B. Graczykowski, E. Chavez-Angel, J. Sebastian Reparaz, M. R. Wagner, C. M. Sotomayor-Torres, S. Xiong, S. Neogi, and D. Donadio, “Nanophononics: state of the art and perspectives,” Eur. Phys. J. B **89**, 15–20 (2016).
24. I. Aharonovich, A. D. Greentree, and S. Prawer, “Diamond photonics,” Nat. Photonics **5**, 397–405 (2011).
25. V. Stojanović, R. J. Ram, M. Popović, S. Lin, S. Moazeni, M. Wade, C. Sun, L. Alloatti, A. Atabaki, F. Pavanello, N. Mehta, and P. Bhargava, “Monolithic silicon-photonic platforms in state-of-the-art CMOS SOI processes [Invited],” Opt. Express **26**, 13106–13121 (2018).
26. B. A. Auld, *Acoustic Fields and Waves in Solids. Volume I & II* (Wiley, 1973).
27. B. Saleh and M. Teich, *Fundamentals of Photonics* (Wiley, 1991).
28. C. Poulton, R. Pant, and B. Eggleton, “Acoustic confinement and stimulated Brillouin scattering in integrated optical waveguides,” J. Opt. Soc. Am. B **30**, 2657–2664 (2013).
29. Y. Liu, N. Dostart, and M. A. Popović, “Toward microphononic circuits on chip: an evaluation of components based on high-contrast evanescent confinement of acoustic waves,” arXiv:1707.06280 (2017).
30. A. Kobyakov, M. Sauer, and D. Chowdhury, “Stimulated Brillouin scattering in optical fibers,” Adv. Opt. Photon. **2**, 1–59 (2010).
31. B. Eggleton, C. Poulton, and R. Pant, “Inducing and harnessing stimulated Brillouin scattering in photonic integrated circuits,” Adv. Opt. Photon. **5**, 536–587 (2013).
32. D. Royer and E. Dieulesaint, *Elastic Waves in Solids I & II* (Springer-Verlag, 2000).
33. M. Aspelmeyer, T. Kippenberg, and F. Marquardt, “Cavity optomechanics,” Rev. Mod. Phys. **86**, 1391–1452 (2014).
34. R. Van Laer, B. Kuyken, D. Van Thourhout, and R. Baets, “Interaction between light and highly confined hypersound in a silicon photonic nanowire,” Nat. Photonics **9**, 199–203 (2015).
35. R. Van Laer, A. Bazin, B. Kuyken, R. Baets, and D. Van Thourhout, “Net on-chip Brillouin gain based on suspended silicon nanowires,” New J. Phys. **17**, 115005 (2015).
36. E. A. Kittlaus, H. Shin, and P. T. Rakich, “Large Brillouin amplification in silicon,” Nat. Photonics **10**, 463–467 (2016).
37. A. A. Oliner, “Waveguide for acoustic surface waves: a review,” Proc. IEEE **64**, 615–627 (1976).
38. E. Ash, R. M. D. L. Rue, and R. F. Humphryes, “Microsound surface waveguides,” IEEE Trans. Microw. Theory Tech. **17**, 882–892 (1969).
39. P. E. Lagasse, “Analysis of silicon ridge waveguides for acoustic surface waves,” in *Microwave Conference* (IEEE, 1973).
40. C. J. Sarabalis, J. T. Hill, and A. H. Safavi-Naeini, “Guided acoustic and optical waves in silicon-on-insulator for Brillouin scattering and optomechanics,” APL Photon. **1**, 071301 (2016).
41. C. J. Sarabalis, Y. D. Dahmani, R. N. Patel, J. T. Hill, and A. H. Safavi-Naeini, “Release-free silicon-on-insulator cavity optomechanics,” Optica **4**, 1147–1150 (2017).
42. H. Shin, W. Qiu, R. Jarecki, J. Cox, R. Olsson, A. Starbuck, Z. Wang, and P. Rakich, “Tailorable stimulated Brillouin scattering in nanoscale silicon waveguides,” Nat. Commun. **4**, 1944 (2013).
43. J. D. Joannopoulos, S. G. Johnson, J. N. Winn, and R. D. Meade, *Photonic Crystals: Molding the Flow of Light* (Princeton University, 2008).
44. X. Sun, X. Zhang, and H. X. Tang, “High-Q silicon optomechanical microdisk resonators at gigahertz frequencies,” Appl. Phys. Lett. **100**, 173116 (2012).
45. M. Maldovan, “Sound and heat revolutions in phononics,” Nature **503**, 209–217 (2013).
46. T. Gorishnyy, C. Ullal, M. Maldovan, G. Fytas, and E. Thomas, “Hypersonic phononic crystals,” Phys. Rev. Lett. **94**, 115501 (2005).
47. V. Laude, A. Khelif, S. Benchabane, M. Wilm, T. Sylvestre, B. Kibler, A. Mussot, J. Dudley, and H. Maillotte, “Phononic band-gap guidance of acoustic modes in photonic crystal fibers,” Phys. Rev. B **71**, 045107 (2005).
48. M. Maldovan and E. L. Thomas, “Simultaneous localization of photons and phonons in two-dimensional periodic structures,” Appl. Phys. Lett. **88**, 251907 (2006).
49. M. Eichenfield, R. Camacho, J. Chan, K. J. Vahala, and O. Painter, “A picogram- and nanometre-scale photonic-crystal optomechanical cavity,” Nature **459**, 550–555 (2009).
50. A. H. Safavi-Naeini and O. Painter, “Design of optomechanical cavities and waveguides on a simultaneous bandgap phononic-photonic crystal slab,” Opt. Express **18**, 14926–14943 (2010).
51. P. E. Lagasse, “Higher-order finite-element analysis of topographic guides supporting elastic surface waves,” J. Acoust. Soc. Am. **53**, 1116–1122 (1973).
52. A. H. Safavi-Naeini, J. T. Hill, S. Meenehan, J. Chan, S. Gröblacher, and O. Painter, “Two-dimensional phononic-photonic band gap optomechanical crystal cavity,” Phys. Rev. Lett. **112**, 153603 (2014).
53. M. Eichenfield, J. Chan, R. M. Camacho, K. J. Vahala, and O. Painter, “Optomechanical crystals,” Nature **462**, 78–82 (2009).
54. F. G. S. Santos, Y. A. V. Espinel, G. O. Luiz, R. S. Benevides, G. S. Wiederhecker, and T. P. Mayer Alegre, “Hybrid confinement of optical and mechanical modes in a bullseye optomechanical resonator,” Opt. Express **25**, 508–529 (2017).
55. J. Chan, T. Alegre, A. H. Safavi-Naeini, J. Hill, A. Krause, S. Gröblacher, M. Aspelmeyer, and O. Painter, “Laser cooling of a nanomechanical oscillator into its quantum ground state,” Nature **478**, 89–92 (2011).

56. J. Gomis-Bresco, D. Navarro-Urrios, M. Oudich, S. El-Jallal, A. Griol, D. Puerto, E. Chavez, Y. Pennec, B. Djafari-Rouhani, F. Alzina, A. Martínez, and C. S. Torres, "A one-dimensional optomechanical crystal with a complete phononic band gap," Nat. Commun. **5**, 4452 (2014).
57. K. Fang, M. H. Matheny, X. Luan, and O. Painter, "Optical transduction and routing of microwave phonons in cavity-optomechanical circuits," Nat. Photonics **10**, 489–496 (2016).
58. K. C. Balram, M. Davanco, J. D. Song, and K. Srinivasan, "Coherent coupling between radio frequency, optical, and acoustic waves in piezo-optomechanical circuits," Nat. Photonics **10**, 1–20 (2015).
59. K. Fang, J. Luo, A. Metelmann, M. H. Matheny, F. Marquardt, A. A. Clerk, and O. Painter, "Generalized non-reciprocity in an optomechanical circuit via synthetic magnetism and reservoir engineering," Nat. Phys. **13**, 465–471 (2017).
60. R. N. Patel, Z. Wang, W. Jiang, C. J. Sarabalis, J. T. Hill, and A. H. Safavi-Naeini, "Single-mode phononic wire," Phys. Rev. Lett. **121**, 040501 (2018).
61. D. Melati, A. Melloni, F. Morichetti, D. Elettronica, I. Bioingegneria, and P. Milano, "Real photonic waveguides: guiding light through imperfections," Adv. Opt. Photon. **6**, 156–224 (2014).
62. M. A. Lemonde, S. Meesala, A. Sipahigil, M. J. Schuetz, M. D. Lukin, M. Loncar, and P. Rabl, "Phonon networks with silicon-vacancy centers in diamond waveguides," Phys. Rev. Lett. **120**, 213603 (2018).
63. M. C. Kuzyk and H. Wang, "Phononic quantum networks of solid-state spins with alternating and frequency-selective waveguides," arXiv:1804.07862 (2018).
64. C. W. Hsu, B. Zhen, J. Lee, S.-L. Chua, S. G. Johnson, J. D. Joannopoulos, and M. Soljačić, "Observation of trapped light within the radiation continuum," Nature **499**, 188–191 (2013).
65. J. Gomis-Bresco, D. Artigas, and L. Torner, "Anisotropy-induced photonic bound states in the continuum," Nat. Photonics **11**, 232–236 (2017).
66. Y. Plotnik, O. Peleg, F. Dreisow, M. Heinrich, S. Nolte, A. Szameit, and M. Segev, "Experimental observation of optical bound states in the continuum," Phys. Rev. Lett. **107**, 28–31 (2011).
67. D. S. Wiersma, P. Bartolini, A. Lagendijk, and R. Righini, "Localization of light in a disordered medium," Nature **390**, 671–673 (1997).
68. M. Segev, Y. Silberberg, and D. Christofilos, "Anderson localization of light," Nat. Photonics **7**, 197–204 (2013).
69. S. H. Mousavi, A. B. Khanikaev, and Z. Wang, "Topologically protected elastic waves in phononic metamaterials," Nat. Commun. **6**, 8682 (2015).
70. M. Hafezi, S. Mittal, J. Fan, A. Migdall, and J. M. Taylor, "Imaging topological edge states in silicon photonics," Nat. Photonics **7**, 1001–1005 (2013).
71. C. Wolff, R. Van Laer, M. J. Steel, B. J. Eggleton, and C. G. Poulton, "Brillouin resonance broadening due to structural variations in nanoscale waveguides," New J. Phys. **18**, 025006 (2016).
72. R. N. Patel, C. J. Sarabalis, W. Jiang, J. T. Hill, and A. H. Safavi-Naeini, "Engineering phonon leakage in nanomechanical resonators," Phys. Rev. Appl. **8**, 041001 (2017).
73. C. J. Sarabalis, R. Van Laer, and A. H. Safavi-Naeini, "Optomechanical antennas for on-chip beam-steering," Opt. Express **26**, 22075–22099 (2018).
74. S. Ghaffari, S. A. Chandorkar, S. Wang, E. J. Ng, C. H. Ahn, V. Hong, Y. Yang, and T. W. Kenny, "Quantum limit of quality factor in silicon micro and nano mechanical resonators," Sci. Rep. **3**, 3244 (2013).
75. E. Chávez-Ángel, R. A. Zarate, J. Gomis-Bresco, F. Alzina, and C. M. Sotomayor Torres, "Modification of Akhieser mechanism in Si nanomembranes and thermal conductivity dependence of the Q-factor of high frequency nanoresonators," Semicond. Sci. Technol. **29**, 124010 (2014).
76. R. O. Behunin, P. Kharel, W. H. Renninger, and P. T. Rakich, "Engineering dissipation with phononic spectral hole burning," Nat. Mater. **16**, 315–321 (2017).
77. T. Ramos, V. Sudhir, K. Stannigel, P. Zoller, and T. J. Kippenberg, "Nonlinear quantum optomechanics via individual intrinsic two-level defects," Phys. Rev. Lett. **110**, 193602 (2013).
78. A. N. Cleland, *Foundations of Nanomechanics: From Solid-State Theory to Device Applications* (Springer-Verlag, 2003).
79. M. Zhang, G. Luiz, S. Shah, G. Wiederhecker, and M. Lipson, "Eliminating anchor loss in optomechanical resonators using elastic wave interference," Appl. Phys. Lett. **105**, 051904 (2014).
80. G. Anetsberger, R. Rivière, A. Schliesser, O. Arcizet, and T. J. Kippenberg, "Ultralow-dissipation optomechanical resonators on a chip," Nat. Photonics **2**, 627–633 (2008).
81. R. Van Laer, R. Baets, and D. Van Thourhout, "Unifying Brillouin scattering and cavity optomechanics," Phys. Rev. A **93**, 053828 (2016).
82. C. Nguyen, "MEMS technology for timing and frequency control," IEEE Trans. Ultrason., Ferroelectr., Freq. Control **54**, 251–270 (2007).
83. K. E. Khosla, G. A. Brawley, M. R. Vanner, and W. P. Bowen, "Quantum optomechanics beyond the quantum coherent oscillation regime," Optica **4**, 1382–1387 (2017).
84. J. S. Bennett and W. P. Bowen, "Rapid mechanical squeezing with pulsed optomechanics," New J. Phys. **20**, 113016 (2018).
85. R. A. Norte, J. P. Moura, and S. Gröblacher, "Mechanical resonators for quantum optomechanics experiments at room temperature," Phys. Rev. Lett. **116**, 1–6 (2016).
86. Y. Tsaturyan, A. Barg, E. S. Polzik, and A. Schliesser, "Ultracoherent nanomechanical resonators via soft clamping and dissipation dilution," Nat. Nanotechnol. **12**, 776–783 (2017).
87. A. H. Ghadimi, S. A. Fedorov, N. J. Engelsen, M. J. Bereyhi, R. Schilling, D. J. Wilson, and T. J. Kippenberg, "Elastic strain engineering for ultralow mechanical dissipation," Science **360**, 764–768 (2018).
88. Q. P. Unterreithmeier, T. Faust, and J. P. Kotthaus, "Damping of nanomechanical resonators," Phys. Rev. Lett. **105**, 027205 (2010).
89. B. D. Hauer, P. H. Kim, C. Doolin, F. Souris, and J. P. Davis, "Two-level system damping in a quasi-one-dimensional optomechanical resonator," Phys. Rev. B **98**, 214303 (2018).
90. W. H. Louisell, A. Yariv, and A. E. Siegman, "Quantum fluctuations and noise in parametric processes. I," Phys. Rev. **124**, 1646–1654 (1961).
91. N. Bloembergen and Y. Shen, "Coupling between vibrations and light waves in Raman laser media," Phys. Rev. Lett. **12**, 504–507 (1964).
92. Y. R. Shen and N. Bloembergen, "Theory of stimulated Brillouin and Raman scattering," Phys. Rev. **137**, A1787–A1805 (1965).
93. A. Yariv, "Quantum theory for parametric interactions of light and hypersound," IEEE J. Quantum Electron. **1**, 28–36 (1965).
94. G. S. Wiederhecker, L. Chen, A. Gondarenko, and M. Lipson, "Controlling photonic structures using optical forces," Nature **462**, 633–636 (2009).
95. J. Rosenberg, Q. Lin, and O. Painter, "Static and dynamic wavelength routing via the gradient optical force," Nat. Photonics **3**, 478–483 (2009).
96. P. Rakich, C. Reinke, R. Camacho, P. Davids, and Z. Wang, "Giant enhancement of stimulated Brillouin scattering in the subwavelength limit," Phys. Rev. X **2**, 011008 (2012).
97. J. Chan, A. H. Safavi-Naeini, J. T. Hill, S. Meenehan, and O. Painter, "Optimized optomechanical crystal cavity with acoustic radiation shield," Appl. Phys. Lett. **101**, 081115 (2012).
98. W. Qiu, P. T. Rakich, H. Shin, H. Dong, M. Soljačić, and Z. Wang, "Stimulated Brillouin scattering in nanoscale silicon step-index waveguides: a general framework of selection rules and calculating SBS gain," Opt. Express **21**, 31402–31419 (2013).
99. C. Wolff, M. J. Steel, B. J. Eggleton, and C. G. Poulton, "Stimulated Brillouin scattering in integrated photonic waveguides: forces, scattering mechanisms and coupled mode analysis," Phys. Rev. A **92**, 013836 (2015).
100. O. Florez, P. F. Jarschel, Y. A. V. Espinel, C. M. B. Cordeiro, T. P. Mayer Alegre, G. S. Wiederhecker, and P. Dainese, "Brillouin scattering self-cancellation," Nat. Commun. **7**, 11759 (2016).
101. R. Leijssen and E. Verhagen, "Strong optomechanical interactions in a sliced photonic crystal nanobeam," Sci. Rep. **5**, 15974 (2015).
102. P. Rabl, "Photon blockade effect in optomechanical systems," Phys. Rev. Lett. **107**, 063601 (2011).
103. J. E. Sipe and M. J. Steel, "A Hamiltonian treatment of stimulated Brillouin scattering in nanoscale integrated waveguides," New J. Phys. **18**, 045004 (2016).
104. H. Zoubi and K. Hammerer, "Optomechanical multimode Hamiltonian for nanophotonic waveguides," Phys. Rev. A **94**, 1–16 (2016).
105. P. Rakich and F. Marquardt, "Quantum theory of continuum optomechanics," New J. Phys. **20**, 045005 (2018).
106. Z. Yu and S. Fan, "Integrated nonmagnetic optical isolators based on photonic transitions," IEEE J. Sel. Top. Quantum Electron. **16**, 459–466 (2010).
107. J. Kim, M. C. Kuzyk, K. Han, H. Wang, and G. Bahl, "Non-reciprocal Brillouin scattering induced transparency," Nat. Phys. **11**, 275–280 (2015).
108. D. B. Sohn, S. Kim, and G. Bahl, "Time-reversal symmetry breaking with acoustic pumping of nanophotonic circuits," Nat. Photonics **12**, 91–97 (2018).

109. E. A. Kittlaus, N. T. Otterstrom, P. Kharel, S. Gertler, and P. T. Rakich, "Non-reciprocal interband Brillouin modulation," Nat. Photonics **12**, 613–619 (2018).
110. A. Seif, W. DeGottardi, K. Esfarjani, and M. Hafezi, "Thermal management and non-reciprocal control of phonon flow via optomechanics," Nat. Commun. **9**, 1207 (2018).
111. V. Peano, C. Brendel, M. Schmidt, and F. Marquardt, "Topological phases of sound and light," Phys. Rev. X **5**, 031011 (2015).
112. R. Van Laer and A. H. Safavi-Naeini, "Enabling strong coupling in nanoscale silicon optomechanical waveguides," in *Conference on Lasers and Electro-Optics* (OSA, 2017), p. FM1F.2.
113. M. Merklein, A. Casas-Bedoya, D. Marpaung, T. Buttner, M. Pagani, B. Morrison, I. Kabakova, and B. Eggleton, "Stimulated Brillouin scattering in photonic integrated circuits: novel applications and devices," IEEE J. Sel. Top. Quantum Electron. **22**, 336–346 (2016).
114. A. H. Safavi-Naeini, J. Chan, J. Hill, T. Alegre, A. Krause, and O. Painter, "Observation of quantum motion of a nanomechanical resonator," Phys. Rev. Lett. **108**, 1–5 (2012).
115. E. Verhagen, S. Deléglise, S. Weis, A. Schliesser, and T. Kippenberg, "Quantum-coherent coupling of a mechanical oscillator to an optical cavity mode," Nature **482**, 63–67 (2012).
116. S. Gröblacher, K. Hammerer, M. Vanner, and M. Aspelmeyer, "Observation of strong coupling between a micromechanical resonator and an optical cavity field," Nature **460**, 724–727 (2009).
117. Y.-D. Wang and A. Clerk, "Using interference for high fidelity quantum state transfer in optomechanics," Phys. Rev. Lett. **108**, 153603 (2012).
118. Y. D. Wang and A. A. Clerk, "Using dark modes for high-fidelity optomechanical quantum state transfer," New J. Phys. **14**, 105010 (2012).
119. J. D. Teufel, D. Li, M. S. Allman, K. Cicak, A. J. Sirois, J. D. Whittaker, and R. W. Simmonds, "Circuit cavity electromechanics in the strong-coupling regime," Nature **471**, 204–208 (2011).
120. J. D. Teufel, T. Donner, D. Li, J. W. Harlow, M. S. Allman, K. Cicak, A. J. Sirois, J. D. Whittaker, K. W. Lehnert, and R. W. Simmonds, "Sideband cooling of micromechanical motion to the quantum ground state," Nature **475**, 359–363 (2011).
121. G. Enzian, M. Szczykulska, J. Silver, L. Del Bino, S. Zhang, I. A. Walmsley, P. Del'Haye, and M. R. Vanner, "Observation of Brillouin optomechanical strong coupling with an 11 GHz mechanical mode," Optica **6**, 7–14 (2019).
122. J. Ma and M. L. Povinelli, "Mechanical Kerr nonlinearities due to bipolar optical forces between deformable silicon waveguides," Opt. Express **19**, 10102–10110 (2011).
123. W. H. P. Pernice, M. Li, and H. X. Tang, "A mechanical Kerr effect in deformable photonic media," Appl. Phys. Lett. **95**, 123507 (2009).
124. S. Aldana, C. Bruder, and A. Nunnenkamp, "Equivalence between an optomechanical system and a Kerr medium," Phys. Rev. A **88**, 1–10 (2013).
125. J. Gea-Banacloche, "Impossibility of large phase shifts via the giant Kerr effect with single-photon wave packets," Phys. Rev. A **81**, 043823 (2010).
126. A. Butsch, C. Conti, F. Biancalana, and P. Russell, "Optomechanical self-channeling of light in a suspended planar dual-nanoweb waveguide," Phys. Rev. Lett. **108**, 093903 (2012).
127. J. T. Hill, A. H. Safavi-Naeini, J. Chan, and O. Painter, "Coherent optical wavelength conversion via cavity optomechanics," Nat. Commun. **3**, 1196 (2012).
128. C. Dong, V. Fiore, M. C. Kuzyk, and H. Wang, "Optomechanical dark mode," Science **338**, 1609–1613 (2012).
129. K. Y. Song, M. G. Herráez, and L. Thévenaz, "Observation of pulse delaying and advancement in optical fibers using stimulated Brillouin scattering," Opt. Express **13**, 82–88 (2005).
130. L. Thévenaz, "Slow and fast light in optical fibres," Nat. Photonics **2**, 474–481 (2008).
131. Y.-C. Chen, S. Kim, and G. Bahl, "Brillouin cooling in a linear waveguide," New J. Phys. **18**, 115004 (2016).
132. N. T. Otterstrom, R. O. Behunin, E. A. Kittlaus, and P. T. Rakich, "Optomechanical cooling in a continuous system," Phys. Rev. X **8**, 041034 (2018).
133. Z. Zhu, D. Gauthier, and R. Boyd, "Stored light in an optical fiber via stimulated Brillouin scattering," Science **318**, 1748–1750 (2007).
134. M. Merklein, B. Stiller, K. Vu, S. J. Madden, and B. J. Eggleton, "A chip-integrated coherent photonic-phononic memory," Nat. Commun. **8**, 574 (2017).
135. M. Merklein, B. Stiller, K. Vu, P. Ma, S. J. Madden, and B. J. Eggleton, "Broad-bandwidth non-reciprocal Brillouin light storage," arXiv:1806.00146 (2018).
136. B. Stiller, M. Merklein, C. Wolff, K. Vu, P. Ma, C. G. Poulton, S. J. Madden, and B. J. Eggleton, "On-chip multi-stage optical delay based on cascaded Brillouin light storage," Opt. Lett. **43**, 4321–4324 (2018).
137. H. Zoubi and K. Hammerer, "Quantum nonlinear optics in optomechanical nanoscale waveguides," Phys. Rev. Lett. **119**, 123602 (2017).
138. E. Romero-Sánchez, W. P. Bowen, M. R. Vanner, K. Xia, and J. Twamley, "Quantum magnetomechanics: towards the ultrastrong coupling regime," Phys. Rev. B **97**, 024109 (2018).
139. J. M. Fink, M. Kalaee, A. Pitanti, R. Norte, L. Heinzle, M. Davanço, K. Srinivasan, and O. Painter, "Quantum electromechanics on silicon nitride nanomembranes," Nat. Commun. **7**, 12396 (2016).
140. P. Arrangoiz-Arriola, E. A. Wollack, M. Pechal, J. D. Witmer, J. T. Hill, and A. H. Safavi-Naeini, "Coupling a superconducting quantum circuit to a phononic crystal defect cavity," Phys. Rev. X **8**, 031007 (2018).
141. P. B. Dieterle, M. Kalaee, J. M. Fink, and O. Painter, "Superconducting cavity electromechanics on a silicon-on-insulator platform," Phys. Rev. Appl. **6**, 014013 (2016).
142. M. Kalaee, M. Mirhosseni, P. B. Dieterle, M. Peruzzo, J. M. Fink, and O. Painter, "Quantum electromechanics of a hypersonic crystal," arXiv:1808.04874 (2018).
143. G. MacCabe, H. Ren, J. Luo, J. Cohen, H. Zhou, A. Sipahigil, M. Mirhosseini, and O. Painter, "Phononic bandgap nano-acoustic cavity with ultralong phonon lifetime," in arXiv:1901.04129 (2019).
144. S. M. Meenehan, J. D. Cohen, G. S. MacCabe, F. Marsili, M. D. Shaw, and O. Painter, "Pulsed excitation dynamics of an optomechanical crystal resonator near its quantum ground state of motion," Phys. Rev. X **5**, 041002 (2015).
145. M. Goryachev, D. L. Creedon, E. N. Ivanov, S. Galliou, R. Bourquin, and M. E. Tobar, "Extremely low-loss acoustic phonons in a quartz bulk acoustic wave resonator," Appl. Phys. Lett. **100**, 243504 (2012).
146. K. E. Grutter, M. I. Davanco, K. Srinivasan, K. A. E. G. Rutter, M. A. I. D. Avanço, and K. A. S. Rinivasan, "Slot-mode optomechanical crystals: a versatile platform for multimode optomechanics," Optica **2**, 994–1001 (2015).
147. Y. Liu, M. Davanço, V. Aksyuk, and K. Srinivasan, "Electromagnetically induced transparency and wideband wavelength conversion in silicon nitride microdisk optomechanical resonators," Phys. Rev. Lett. **110**, 223603 (2013).
148. S. Galliou, M. Goryachev, R. Bourquin, P. Abbé, J. P. Aubry, and M. E. Tobar, "Extremely low loss phonon-trapping cryogenic acoustic cavities for future physical experiments," Sci. Rep. **3**, 2132 (2013).
149. S. M. Meenehan, J. D. Cohen, S. Gröblacher, J. T. Hill, A. H. Safavi-Naeini, M. Aspelmeyer, and O. Painter, "Silicon optomechanical crystal resonator at millikelvin temperatures," Phys. Rev. A **90**, 1–5 (2014).
150. A. N. Cleland and M. R. Geller, "Superconducting qubit storage and entanglement with nanomechanical resonators," Phys. Rev. Lett. **93**, 1–4 (2004).
151. R. Rivière, S. Deléglise, S. Weis, E. Gavartin, O. Arcizet, A. Schliesser, and T. J. Kippenberg, "Optomechanical sideband cooling of a micromechanical oscillator close to the quantum ground state," Phys. Rev. A **83**, 1–9 (2011).
152. A. Schliesser, O. Arcizet, R. Rivière, G. Anetsberger, and T. J. Kippenberg, "Resolved-sideband cooling and position measurement of a micromechanical oscillator close to the Heisenberg uncertainty limit," Nat. Phys. **5**, 509–514 (2009).
153. D. J. Wilson, V. Sudhir, N. Piro, R. Schilling, A. Ghadimi, and T. J. Kippenberg, "Measurement-based control of a mechanical oscillator at its thermal decoherence rate," Nature **524**, 325–329 (2015).
154. A. H. Safavi-Naeini, S. Gröblacher, J. T. Hill, J. Chan, M. Aspelmeyer, and O. Painter, "Squeezed light from a silicon micromechanical resonator," Nature **500**, 185–189 (2013).
155. A. G. Krause, J. T. Hill, M. Ludwig, A. H. Safavi-Naeini, J. Chan, F. Marquardt, and O. Painter, "Nonlinear radiation pressure dynamics in an optomechanical crystal," Phys. Rev. Lett. **115**, 1–5 (2015).
156. X. Sun, X. Zhang, M. Poot, C. Xiong, and H. X. Tang, "A superhigh-frequency optoelectromechanical system based on a slotted photonic crystal cavity," Appl. Phys. Lett. **101**, 221116 (2012).
157. C. Xiong, L. Fan, X. Sun, and H. X. Tang, "Cavity piezooptomechanics: piezoelectrically excited, optically transduced optomechanical resonators," Appl. Phys. Lett. **102**, 1–5 (2013).

158. E. A. Kittlaus, N. T. Otterstrom, and P. T. Rakich, "On-chip inter-modal Brillouin scattering," Nat. Commun. **8**, 15819 (2017).
159. T. P. Purdy, R. W. Peterson, P.-L. Yu, and C. A. Regal, "Cavity optomechanics with Si_3N_4 membranes at cryogenic temperatures," New J. Phys. **14**, 115021 (2012).
160. I. A. Williamson, S. H. Mousavi, and Z. Wang, "Large cavity-optomechanical coupling with graphene at infrared and terahertz frequencies," ACS Photon. **3**, 2353–2361 (2016).
161. A. J. Weinstein, C. U. Lei, E. E. Wollman, J. Suh, A. Metelmann, A. A. Clerk, and K. C. Schwab, "Observation and interpretation of motional sideband asymmetry in a quantum electromechanical device," Phys. Rev. X **4**, 041003 (2014).
162. E. E. Wollman, C. U. Lei, A. J. Weinstein, J. Suh, A. Kronwald, F. Marquardt, A. Clerk, and K. C. Schwab, "Quantum squeezing of motion in a mechanical resonator," Science **349**, 952–955 (2015).
163. J.-M. Pirkkalainen, E. Damskägg, M. Brandt, F. Massel, and M. A. Sillanpää, "Squeezing of quantum noise of motion in a micromechanical resonator," Phys. Rev. Lett. **115**, 243601 (2015).
164. H. Rong, S. Xu, Y.-H. Kuo, V. Sih, O. Cohen, O. Raday, and M. Paniccia, "Low-threshold continuous-wave Raman silicon laser," Nat. Photonics **1**, 232–237 (2007).
165. R. Pant, D. Marpaung, I. V. Kabakova, B. Morrison, C. G. Poulton, and B. J. Eggleton, "On-chip stimulated Brillouin scattering for microwave signal processing and generation," Laser Photon. Rev. **8**, 653–666 (2014).
166. R. Pant, C. G. Poulton, D.-Y. Choi, H. Mcfarlane, S. Hile, E. Li, L. Thevenaz, B. Luther-Davies, S. J. Madden, and B. J. Eggleton, "On-chip stimulated Brillouin scattering," Opt. Express **19**, 8285–8290 (2011).
167. B. Kuyken, H. Ji, S. Clemmen, S. K. Selvaraja, H. Hu, M. Pu, M. Galili, P. Jeppesen, G. Morthier, S. Massar, L. K. Oxenløwe, G. Roelkens, and R. Baets, "Nonlinear properties of and nonlinear processing in hydrogenated amorphous silicon waveguides," Opt. Express **19**, B146–B153 (2011).
168. M. S. Kang, A. Nazarkin, A. Brenn, and P. S. T. Russell, "Tightly trapped acoustic phonons in photonic crystal fibres as highly nonlinear artificial Raman oscillators," Nat. Phys. **5**, 276–280 (2009).
169. K. S. Abedin, "Brillouin amplification and lasing in a single-mode As_2Se_3 chalcogenide fiber," Opt. Lett. **31**, 1615–1617 (2006).
170. A. Butsch, J. Koehler, R. Noskov, and P. Russell, "CW-pumped single-pass frequency comb generation by resonant optomechanical nonlinearity in dual-nanoweb fiber," Optica **1**, 158–164 (2014).
171. B. Kuyken, F. Leo, S. Clemmen, U. Dave, R. Van Laer, T. Ideguchi, H. Zhao, X. Liu, J. Safioui, S. Coen, S. Gorza, S. K. Selvaraja, S. Massar, R. M. Osgood, P. Verheyen, J. Van Campenhout, R. Baets, W. J. Green, and G. Roelkens, "Nonlinear optical interactions in silicon waveguides," Nanophotonics **6**, 377–392 (2016).
172. M. K. Schmidt, C. G. Poulton, G. Z. Mashanovich, G. T. Reed, B. J. Eggleton, and M. J. Steel, "Suspended mid-infrared waveguides for stimulated Brillouin scattering," arXiv:1811.02749 (2018).
173. R. Van Laer, C. J. Sarabalis, R. Baets, D. Van Thourhout, and A. H. Safavi-Naeini, "Thermal Brillouin noise observed in silicon optomechanical waveguide," J. Opt. **19**, 044002 (2017).
174. C. Wolff, M. J. Steel, B. J. Eggleton, and C. G. Poulton, "Acoustic build-up in on-chip stimulated Brillouin scattering," Sci. Rep. **5**, 13656 (2015).
175. A. Choudhary, B. Morrison, I. Aryanfar, S. Shahnia, M. Pagani, Y. Liu, K. Vu, S. Madden, D. Marpaung, and B. J. Eggleton, "Advanced integrated microwave signal processing with giant on-chip Brillouin gain," J. Lightwave Technol. **35**, 846–854 (2017).
176. J. R. Koehler, R. E. Noskov, A. A. Sukhorukov, A. Butsch, D. Novoa, and P. St. J. Russell, "Resolving the mystery of milliwatt-threshold optomechanical self-oscillation in dual-nanoweb fiber," APL Photon. **1**, 056101 (2016).
177. A. D. O'Connell, M. Hofheinz, M. Ansmann, R. C. Bialczak, M. Lenander, E. Lucero, M. Neeley, D. Sank, H. Wang, M. Weides, J. Wenner, J. M. Martinis, and A. N. Cleland, "Quantum ground state and single-phonon control of a mechanical resonator," Nature **464**, 697–703 (2010).
178. A. Schliesser, R. Rivière, G. Anetsberger, O. Arcizet, and T. J. Kippenberg, "Resolved-sideband cooling of a micromechanical oscillator," Nat. Phys. **4**, 415–419 (2008).
179. E. Gil-Santos, C. Baker, D. T. Nguyen, W. Hease, C. Gomez, A. Lemaître, S. Ducci, G. Leo, and I. Favero, "High-frequency nano-optomechanical disk resonators in liquids," Nat. Nanotechnol. **10**, 810–816 (2015).
180. P. Kharel, Y. Chu, M. Power, W. H. Renninger, R. J. Schoelkopf, and P. T. Rakich, "Ultra-high- Q phononic resonators on-chip at cryogenic temperatures," APL Photon. **3**, 066101 (2018).
181. L. Neumeier, T. E. Northup, and D. E. Chang, "Reaching the optomechanical strong-coupling regime with a single atom in a cavity," Phys. Rev. A **97**, 1–8 (2018).
182. G. Bahl, M. Tomes, F. Marquardt, and T. Carmon, "Observation of spontaneous Brillouin cooling," Nat. Phys. **8**, 203–207 (2012).
183. K. L. Ekinci and M. L. Roukes, "Nanoelectromechanical systems," Rev. Sci. Instrum. **76**, 061101 (2005).
184. A. Nunnenkamp, K. Børkje, and S. M. Girvin, "Single-photon optomechanics," Phys. Rev. Lett. **107**, 063602 (2011).
185. P. Kómár, S. D. Bennett, K. Stannigel, S. J. M. Habraken, P. Rabl, P. Zoller, and M. D. Lukin, "Single-photon nonlinearities in two-mode optomechanics," Phys. Rev. A **87**, 013839 (2013).
186. M. Ludwig, A. H. Safavi-Naeini, O. Painter, and F. Marquardt, "Enhanced quantum nonlinearities in a two-mode optomechanical system," Phys. Rev. Lett. **109**, 1–5 (2012).
187. A. Kronwald and F. Marquardt, "Optomechanically induced transparency in the nonlinear quantum regime," Phys. Rev. Lett. **111**, 133601 (2013).
188. Y. Okawachi, M. S. Bigelow, J. E. Sharping, Z. Zhu, A. Schweinsberg, D. J. Gauthier, R. W. Boyd, and A. L. Gaeta, "Tunable all-optical delays via Brillouin slow light in an optical fiber," Phys. Rev. Lett. **94**, 153902 (2005).
189. D. J. Brod and J. Combes, "Passive CPHASE gate via cross-Kerr nonlinearities," Phys. Rev. Lett. **117**, 1–6 (2016).
190. D. J. Brod, J. Combes, and J. Gea-Banacloche, "Two photons co- and counterpropagating through N cross-Kerr sites," Phys. Rev. A **94**, 023833 (2016).
191. J. Gea-Banacloche and N. Német, "Conditional phase gate using an optomechanical resonator," Phys. Rev. A **89**, 1–13 (2014).
192. K. Schneider and P. Seidler, "Strong optomechanical coupling in a slotted photonic crystal nanobeam cavity with an ultrahigh quality factor-to-mode volume ratio," Opt. Express **24**, 13850–13865 (2016).
193. R. Van Laer, B. Kuyken, D. Van Thourhout, and R. Baets, "Analysis of enhanced stimulated Brillouin scattering in silicon slot waveguides," Opt. Lett. **39**, 1242–1245 (2014).
194. C. Baker, W. Hease, D.-T. Nguyen, A. Andronico, S. Ducci, G. Leo, and I. Favero, "Photoelastic coupling in gallium arsenide optomechanical disk resonators," Opt. Express **22**, 14072–14086 (2014).
195. M.-A. Lemonde, N. Didier, and A. Clerk, "Enhanced nonlinear interactions in quantum optomechanics via mechanical amplification," Nat. Commun. **7**, 11338 (2016).
196. Z. Wang and A. H. Safavi-Naeini, "Enhancing a slow and weak optomechanical nonlinearity with delayed quantum feedback," Nat. Commun. **8**, 15886 (2017).
197. A. Xuereb, C. Genes, and A. Dantan, "Strong coupling and long-range collective interactions in optomechanical arrays," Phys. Rev. Lett. **109**, 223601 (2012).
198. C. Gärtner, J. P. Moura, W. Haaxman, R. A. Norte, and S. Gröblacher, "Integrated optomechanical arrays of two high reflectivity SiN membranes," arXiv:1809.06372 (2018).
199. J. Roels, I. De Vlaminck, L. Lagae, B. Maes, D. Van Thourhout, and R. Baets, "Tunable optical forces between nanophotonic waveguides," Nat. Nanotechnol. **4**, 510–513 (2009).
200. D. Van Thourhout, T. Spuesens, S. K. Selvaraja, L. Liu, G. Roelkens, R. Kumar, G. Morthier, P. Rojo-Romeo, F. Mandorlo, P. Regreny, O. Raz, C. Kopp, and L. Grenouillet, "Nanophotonic devices for optical interconnect," IEEE J. Sel. Top. Quantum Electron. **16**, 1363–1375 (2010).
201. C. Poulton, R. Pant, A. Byrnes, and S. Fan, "Design for broadband on-chip isolator using stimulated Brillouin scattering in dispersion-engineered chalcogenide waveguides," Opt. Express **20**, 21235 (2012).
202. M. Tsang, "Cavity quantum electro-optics," Phys. Rev. A **81**, 063837 (2010).
203. M. Tsang, "Cavity quantum electro-optics. II. Input-output relations between traveling optical and microwave fields," Phys. Rev. A **84**, 043845 (2011).
204. C. Wang, M. Zhang, B. Stern, M. Lipson, and M. Lončar, "Nanophotonic lithium niobate electro-optic modulators," Opt. Express **26**, 1547–1555 (2018).
205. L. Midolo, A. Schliesser, and A. Fiore, "Nano-opto-electro-mechanical systems," Nat. Nanotechnol. **13**, 11–18 (2018).

206. M. Poot and H. S. J. van der Zant, "Mechanical systems in the quantum regime," Phys. Rep. **511**, 11–18 (2012).
207. K. Van Acoleyen, J. Roels, P. Mechet, T. Claes, D. Van Thourhout, and R. Baets, "Ultracompact phase modulator based on a cascade of NEMS-operated slot waveguides fabricated in silicon-on-insulator," IEEE Photon. J. **4**, 779–788 (2012).
208. A. Pitanti, J. M. Fink, A. H. Safavi-Naeini, J. T. Hill, C. U. Lei, A. Tredicucci, and O. Painter, "Strong opto-electro-mechanical coupling in a silicon photonic crystal cavity," Opt. Express **23**, 3196–3208 (2015).
209. M. Winger, T. D. Blasius, T. P. Mayer Alegre, A. H. Safavi-Naeini, S. Meenehan, J. Cohen, S. Stobbe, and O. Painter, "A chip-scale integrated cavity-electro-optomechanics platform," Opt. Express **19**, 24905–24921 (2011).
210. W. Jin, R. G. Polcawich, P. A. Morton, and J. E. Bowers, "Phase tuning by length contraction," Opt. Express **26**, 3174–3187 (2018).
211. C. Errando-Herranz, F. Niklaus, G. Stemme, and K. B. Gylfason, "Low-power microelectromechanically tunable silicon photonic ring resonator add-drop filter," Opt. Lett. **40**, 3556–3559 (2015).
212. T. J. Seok, N. Quack, S. Han, R. S. Muller, and M. C. Wu, "Large-scale broadband digital silicon photonic switches with vertical adiabatic couplers," Optica **3**, 64–70 (2016).
213. D. A. B. Miller, "Self-aligning universal beam coupler," Opt. Express **21**, 6360–6370 (2013).
214. D. A. B. Miller, "Perfect optics with imperfect components," Optica **2**, 747–750 (2015).
215. J. Carolan, C. Harrold, C. Sparrow, E. Martin-Lopez, N. J. Russell, J. W. Silverstone, P. J. Shadbolt, N. Matsuda, M. Oguma, M. Itoh, G. D. Marshall, M. G. Thompson, J. C. F. Matthews, T. Hashimoto, J. L. O'Brien, and A. Laing, "Universal linear optics," Science **349**, 711–716 (2015).
216. Y. Shen, N. C. Harris, S. Skirlo, M. Prabhu, T. Baehr-Jones, M. Hochberg, X. Sun, S. Zhao, H. Larochelle, D. Englund, and M. Soljačić, "Deep learning with coherent nanophotonic circuits," Nat. Photonics **11**, 441–446 (2017).
217. T. Rudolph, "Why I am optimistic about the silicon-photonic route to quantum computing," APL Photon. **2**, 030901 (2017).
218. P. J. Shadbolt, M. R. Verde, A. Peruzzo, A. Politi, A. Laing, M. Lobino, J. C. F. Matthews, M. G. Thompson, and J. L. O'Brien, "Generating, manipulating and measuring entanglement and mixture with a reconfigurable photonic circuit," Nat. Photonics **6**, 45–49 (2012).
219. X. Qiang, X. Zhou, J. Wang, C. M. Wilkes, T. Loke, S. O'Gara, L. Kling, G. D. Marshall, R. Santagati, T. C. Ralph, J. B. Wang, J. L. O'Brien, M. G. Thompson, and J. C. F. Matthews, "Large-scale silicon quantum photonics implementing arbitrary two-qubit processing," Nat. Photonics **12**, 534–539 (2018).
220. C. Papon, X. Zhou, H. Thyrrestrup, Z. Liu, S. Stobbe, R. Schott, A. D. Wieck, A. Ludwig, P. Lodahl, and L. Midolo, "Nanomechanical single-photon routing," arXiv:1811.10962 (2018).
221. C. Errando-Herranz, N. L. Thomas, and K. B. Gylfason, "Low-power optical beam steering by microelectromechanical waveguide gratings," arXiv:1809.04483 (2018).
222. D. Jalas, A. Petrov, M. Eich, W. Freude, S. Fan, Z. Yu, R. Baets, M. Popović, A. Melloni, J. D. Joannopoulos, M. Vanwolleghem, C. R. Doerr, and H. Renner, "What is—and what is not—an optical isolator," Nat. Photonics **7**, 579–582 (2013).
223. D. L. Sounas and A. Alù, "Non-reciprocal photonics based on time modulation," Nat. Photonics **11**, 774–783 (2017).
224. M.-A. Miri, F. Ruesink, E. Verhagen, and A. Alù, "Optical nonreciprocity based on optomechanical coupling," Phys. Rev. Appl. **7**, 064014 (2017).
225. E. Verhagen and A. Alù, "Optomechanical nonreciprocity," Nat. Phys. **13**, 922–924 (2017).
226. L. Ranzani, S. Kotler, A. J. Sirois, M. P. DeFeo, M. Castellanos-Beltran, K. Cicak, L. R. Vale, and J. Aumentado, "Wideband isolation by frequency conversion in a Josephson-junction transmission line," Phys. Rev. Appl. **8**, 054035 (2017).
227. E. A. Kittlaus, P. Kharel, N. T. Otterstrom, Z. Wang, and P. T. Rakich, "RF-photonic filters via on-chip photonic-phononic emit-receive operations," J. Lightwave Technol. **36**, 2803–2809 (2018).
228. C. Dong, Z. Shen, C.-L. Zou, Y.-L. Zhang, W. Fu, and G.-C. Guo, "Brillouin-scattering-induced transparency and non-reciprocal light storage," Nat. Commun. **6**, 6193 (2015).
229. Q. P. Unterreithmeier, E. M. Weig, and J. P. Kotthaus, "Universal transduction scheme for nanomechanical systems based on dielectric forces," Nature **458**, 1001–1004 (2009).
230. D. Weinstein and S. Bhave, "Internal dielectric transduction in bulk-mode resonators," J. Microelectromech. Syst. **18**, 1401–1408 (2009).
231. D. Weinstein and S. A. Bhave, "The resonant body transistor," Nano Lett. **10**, 1234–1237 (2010).
232. R. Van Laer, R. N. Patel, T. P. McKenna, J. D. Witmer, and A. H. Safavi-Naeini, "Electrical driving of X-band mechanical waves in a silicon photonic circuit," APL Photon. **3**, 086102 (2018).
233. M. M. de Lima, M. Beck, R. Hey, and P. V. Santos, "Compact Mach-Zehnder acousto-optic modulator," Appl. Phys. Lett. **89**, 121104 (2006).
234. S. A. Tadesse and M. Li, "Sub-optical wavelength acoustic wave modulation of integrated photonic resonators at microwave frequencies," Nat. Commun. **5**, 5402 (2014).
235. C. Xiong, L. Fan, X. Sun, and H. X. Tang, "Cavity piezooptomechanics: piezoelectrically excited, optically transduced optomechanical resonators," Appl. Phys. Lett. **102**, 021110 (2013).
236. K. Alexander, J. P. George, J. Verbist, K. Neyts, B. Kuyken, D. Van Thourhout, and J. Beeckman, "Nanophotonic Pockels modulators on a silicon nitride platform," Nat. Commun. **9**, 3444 (2018).
237. P. O. Weigel, J. Zhao, K. Fang, H. Al-Rubaye, D. Trotter, D. Hood, J. Mudrick, C. Dallo, A. T. Pomerene, A. L. Starbuck, C. T. DeRose, A. L. Lentine, G. Rebeiz, and S. Mookherjea, "Bonded thin film lithium niobate modulator on a silicon photonics platform exceeding 100 GHz 3-dB electrical modulation bandwidth," Opt. Express **26**, 23728–23739 (2018).
238. A. Siddiqui, R. H. Olsson, and M. Eichenfield, "Lamb wave focusing transducer for efficient coupling to wavelength-scale structures in thin piezoelectric films," J. Microelectromech. Syst. **27**, 1054–1070 (2018).
239. C. Gorecki, F. Chollet, E. Bonnotte, and H. Kawakatsu, "Silicon-based integrated interferometer with phase modulation driven by surface acoustic waves," Opt. Lett. **22**, 1784–1786 (1997).
240. O. Marshall, M. Hsu, Z. Wang, B. Kunert, C. Koos, and D. Van Thourhout, "Heterogeneous integration on silicon photonics," Proc. IEEE **106**, 2258–2269 (2018).
241. Z. Yu and S. Fan, "Optical isolation based on nonreciprocal phase shift induced by interband photonic transitions," Appl. Phys. Lett. **94**, 171116 (2009).
242. K. Fang, Z. Yu, and S. Fan, "Realizing effective magnetic field for photons by controlling the phase of dynamic modulation," Nat. Photonics **6**, 782–787 (2012).
243. Y. Shi, S. Han, and S. Fan, "Optical circulation and isolation based on indirect photonic transitions of guided resonance modes," ACS Photon. **4**, 1639–1645 (2017).
244. N. Dostart, Y. Ehrlichman, C. Gentry, and M. Popovic, "Energy-efficient active integrated photonic isolators using electrically driven acoustic waves," arXiv:1811.01052 (2018).
245. S. Sun, H. Kim, G. S. Solomon, and E. Waks, "Strain tuning of a quantum dot strongly coupled to a photonic crystal cavity," Appl. Phys. Lett. **103**, 151102 (2013).
246. D. Lee, K. W. Lee, J. V. Cady, P. Ovartchaiyapong, and A. C. B. Jayich, "Topical review: spins and mechanics in diamond," J. Opt. **19**, 033001 (2017).
247. M. S. J. Barson, P. Peddibhotla, P. Ovartchaiyapong, K. Ganesan, R. L. Taylor, M. Gebert, Z. Mielens, B. Koslowski, D. A. Simpson, L. P. McGuinness, J. McCallum, S. Prawer, S. Onoda, T. Ohshima, A. C. Bleszynski Jayich, F. Jelezko, N. B. Manson, and M. W. Doherty, "Nanomechanical sensing using spins in diamond," Nano Lett. **17**, 1496–1503 (2017).
248. Y. I. Sohn, S. Meesala, B. Pingault, H. A. Atikian, J. Holzgrafe, M. Gündoğan, C. Stavrakas, M. J. Stanley, A. Sipahigil, J. Choi, M. Zhang, J. L. Pacheco, J. Abraham, E. Bielejec, M. D. Lukin, M. Atatüre, and M. Lončar, "Controlling the coherence of a diamond spin qubit through its strain environment," Nat. Commun. **9**, 17–22 (2018).
249. R. W. Andrews, R. W. Peterson, T. P. Purdy, K. Cicak, R. W. Simmonds, C. A. Regal, and K. W. Lehnert, "Bidirectional and efficient conversion between microwave and optical light," Nat. Phys. **10**, 321–326 (2014).
250. M. Pechal, P. Arrangoiz-Arriola, and A. H. Safavi-Naeini, "Superconducting circuit quantum computing with nanomechanical resonators as storage," Quantum Sci. Technol. **4**, 015006 (2018).
251. J. Bochmann, A. Vainsencher, D. D. Awschalom, and A. N. Cleland, "Nanomechanical coupling between microwave and optical photons," Nat. Phys. **9**, 712–716 (2013).
252. A. H. Safavi-Naeini, T. P. Mayer Alegre, J. Chan, M. Eichenfield, M. Winger, Q. Lin, J. T. Hill, D. E. Chang, and O. Painter,

"Electromagnetically induced transparency and slow light with optomechanics," Nature **472**, 69–73 (2011).
253. T. Bagci, A. Simonsen, S. Schmid, L. G. Villanueva, E. Zeuthen, J. Appel, J. M. Taylor, A. Sørensen, K. Usami, A. Schliesser, and E. S. Polzik, "Optical detection of radio waves through a nanomechanical transducer," Nature **507**, 81–85 (2014).
254. A. Rueda, F. Sedlmeir, M. C. Collodo, U. Vogl, B. Stiller, G. Schunk, D. V. Strekalov, C. Marquardt, J. M. Fink, O. Painter, G. Leuchs, and H. G. L. Schwefel, "Efficient microwave to optical photon conversion: an electro-optical realization," Optica **3**, 597–604 (2016).
255. A. Vainsencher, K. J. Satzinger, G. A. Peairs, and A. N. Cleland, "Bi-directional conversion between microwave and optical frequencies in a piezoelectric optomechanical device," Appl. Phys. Lett. **109**, 033107 (2016).
256. J. Preskill, "Quantum computing and the entanglement frontier," arXiv:1203.5813 (2012).
257. J. Preskill, "Quantum computing in the NISQ era and beyond," arXiv:1801.00862 (2018).
258. M. H. Devoret and R. J. Schoelkopf, "Superconducting circuits for quantum information: an outlook," Science **339**, 1169–1174 (2013).
259. R. Barends, J. Kelly, A. Megrant, A. Veitia, D. Sank, E. Jeffrey, T. C. White, J. Mutus, A. G. Fowler, B. Campbell, Y. Chen, Z. Chen, B. Chiaro, A. Dunsworth, C. Neill, P. O'Malley, P. Roushan, A. Vainsencher, J. Wenner, A. N. Korotkov, A. N. Cleland, and J. M. Martinis, "Superconducting quantum circuits at the surface code threshold for fault tolerance," Nature **508**, 500–503 (2014).
260. A. J. Keller, P. B. Dieterle, M. Fang, B. Berger, J. M. Fink, and O. Painter, "Al transmon qubits on silicon-on-insulator for quantum device integration," Appl. Phys. Lett. **111**, 042603 (2017).
261. S. Krinner, S. Storz, P. Kurpiers, P. Magnard, J. Heinsoo, R. Keller, J. Lütolf, C. Eichler, and A. Wallraff, "Engineering cryogenic setups for 100-qubit scale superconducting circuit systems," arXiv:1806.07862 (2018).
262. C. Neill, P. Roushan, K. Kechedzhi, S. Boixo, S. V. Isakov, V. Smelyanskiy, A. Megrant, B. Chiaro, A. Dunsworth, K. Arya, R. Barends, B. Burkett, Y. Chen, Z. Chen, A. Fowler, B. Foxen, M. Giustina, R. Graff, E. Jeffrey, T. Huang, J. Kelly, P. Klimov, E. Lucero, J. Mutus, M. Neeley, C. Quintana, D. Sank, A. Vainsencher, J. Wenner, T. C. White, H. Neven, and J. M. Martinis, "A blueprint for demonstrating quantum supremacy with superconducting qubits," Science **360**, 195–199 (2018).
263. B. Vermersch, P.-O. Guimond, H. Pichler, and P. Zoller, "Quantum state transfer via noisy photonic and phononic waveguides," Phys. Rev. Lett. **118**, 133601 (2017).
264. Z.-L. Xiang, M. Zhang, L. Jiang, and P. Rabl, "Intracity quantum communication via thermal microwave networks," Phys. Rev. X **7**, 011035 (2017).
265. H. J. Kimble, "The quantum internet," Nature **453**, 1023–1030 (2008).
266. C. R. Monroe, R. J. Schoelkopf, and M. D. Lukin, "Quantum connections," Sci. Am. **314**, 50–57 (2016).
267. M. Pechal and A. H. Safavi-Naeini, "Millimeter-wave interconnects for microwave-frequency quantum machines," Phys. Rev. A **96**, 042305 (2017).
268. L. Fan, C.-L. Zou, R. Cheng, X. Guo, X. Han, Z. Gong, S. Wang, and H. X. Tang, "Superconducting cavity electro-optics: a platform for coherent photon conversion between superconducting and photonic circuits," Sci. Adv. **4**, eaar4994 (2018).
269. C. Kieninger, Y. Kutuvantavida, D. L. Elder, S. Wolf, H. Zwickel, M. Blaicher, J. N. Kemal, M. Lauermann, S. Randel, W. Freude, L. R. Dalton, and C. Koos, "Ultra-high electro-optic activity demonstrated in a silicon-organic hybrid modulator," Optica **5**, 739–748 (2018).
270. Y. Chu, P. Kharel, W. H. Renninger, L. D. Burkhart, L. Frunzio, P. T. Rakich, and R. J. Schoelkopf, "Quantum acoustics with superconducting qubits," Science **358**, 199–202 (2017).
271. F. Lecocq, J. D. Teufel, J. Aumentado, and R. W. Simmonds, "Resolving the vacuum fluctuations of an optomechanical system using an artificial atom," Nat. Phys. **11**, 635–639 (2015).
272. P. Arrangoiz-Arriola and A. H. Safavi-Naeini, "Engineering interactions between superconducting qubits and phononic nanostructures," Phys. Rev. A **94**, 063864 (2016).
273. M. V. Gustafsson, T. Aref, A. F. Kockum, M. K. Ekstrom, G. Johansson, and P. Delsing, "Propagating phonons coupled to an artificial atom," Science **346**, 207–211 (2014).
274. M. K. Ekström, T. Aref, J. Runeson, J. Björck, I. Boström, and P. Delsing, "Surface acoustic wave unidirectional transducers for quantum applications," Appl. Phys. Lett. **110**, 073105 (2017).
275. I. Mahboob and H. Yamaguchi, "Bit storage and bit flip operations in an electromechanical oscillator," Nat. Nanotechnol. **3**, 275–279 (2008).
276. Y. Chu, P. Kharel, T. Yoon, L. Frunzio, P. T. Rakich, and R. J. Schoelkopf, "Climbing the phonon Fock state ladder," arXiv:1804.07426 (2018).
277. K. E. Khosla, M. R. Vanner, N. Ares, and E. A. Laird, "Displacemon electromechanics: how to detect quantum interference in a nanomechanical resonator," Phys. Rev. X **8**, 021052 (2017).
278. J. J. Viennot, X. Ma, and K. W. Lehnert, "Phonon-number-sensitive electromechanics," Phys. Rev. Lett. **121**, 183601 (2018).
279. E. J. Davis, Z. Wang, A. H. Safavi-Naeini, and M. H. Schleier-Smith, "Painting nonclassical states of spin or motion with shaped single photons," Phys. Rev. Lett. **121**, 123602 (2018).
280. R. Riedinger, S. Hong, R. A. Norte, J. A. Slater, J. Shang, A. G. Krause, V. Anant, M. Aspelmeyer, and S. Gröblacher, "Non-classical correlations between single photons and phonons from a mechanical oscillator," Nature **530**, 1–12 (2015).
281. S. Hong, R. Riedinger, I. Marinković, A. Wallucks, S. G. Hofer, R. A. Norte, M. Aspelmeyer, and S. Gröblacher, "Hanbury Brown and Twiss interferometry of single phonons from an optomechanical resonator," Science **358**, 203–206 (2017).
282. J. Capmany and D. Novak, "Microwave photonics combines two worlds," Nat. Photonics **1**, 319–330 (2007).
283. D. Marpaung, B. Morrison, R. Pant, and B. J. Eggleton, "Frequency agile microwave photonic notch filter with anomalously high stopband rejection," Opt. Lett. **38**, 4300–4303 (2013).
284. D. Marpaung, J. Yao, and J. Capmany, "Integrated microwave photonics," Nature Photon. **13**, 80–90 (2019).
285. Y. Liu, A. Choudhary, D. Marpaung, and B. J. Eggleton, "Chip-based Brillouin processing for phase control of RF signals," IEEE J. Quantum Electron. **54**, 1–13 (2018).
286. A. Byrnes, R. Pant, E. Li, D.-Y. Choi, C. G. Poulton, S. Fan, S. Madden, B. Luther-Davies, and B. J. Eggleton, "Photonic chip based tunable and reconfigurable narrowband microwave photonic filter using stimulated Brillouin scattering," Opt. Express **20**, 18836–18845 (2012).
287. B. Morrison, D. Marpaung, R. Pant, E. Li, D.-Y. Choi, S. Madden, B. Luther-Davies, and B. J. Eggleton, "Tunable microwave photonic notch filter using on-chip stimulated Brillouin scattering," Opt. Commun. **313**, 85–89 (2014).
288. D. Marpaung, B. Morrison, M. Pagani, R. Pant, D. Choi, B. Davies, S. Madden, and B. Eggleton, "Low-power, chip-based stimulated Brillouin scattering microwave photonic filter with ultrahigh selectivity," Optica **2**, 76–83 (2015).
289. A. Casas-Bedoya, B. Morrison, M. Pagani, D. Marpaung, and B. J. Eggleton, "Tunable narrowband microwave photonic filter created by stimulated Brillouin scattering from a silicon nanowire," Opt. Lett. **40**, 4154–4157 (2015).
290. H. Shin, J. A. Cox, R. Jarecki, A. Starbuck, Z. Wang, and P. T. Rakich, "Control of coherent information via on-chip photonic-phononic emitter-receivers," Nat. Commun. **6**, 6427 (2015).
291. A. Zadok, A. Eyal, and M. Tur, "Gigahertz-wide optically reconfigurable filters using stimulated Brillouin scattering," J. Lightwave Technol. **25**, 2168–2174 (2007).
292. M. Merklein, B. Stiller, I. V. Kabakova, U. S. Mutugala, K. Vu, S. J. Madden, B. J. Eggleton, and R. Slavík, "Widely tunable, low phase noise microwave source based on a photonic chip," Opt. Lett. **41**, 4633–4636 (2016).
293. J. Li, H. Lee, T. Chen, and K. J. Vahala, "Characterization of a high coherence, Brillouin microcavity laser on silicon," Opt. Express **20**, 20170–20180 (2012).
294. M. G. Suh, Q. F. Yang, and K. J. Vahala, "Phonon-limited-linewidth of Brillouin lasers at cryogenic temperatures," Phys. Rev. Lett. **119**, 1–6 (2017).
295. J. Li, M.-G. Suh, and K. Vahala, "Microresonator Brillouin gyroscope," Optica **4**, 346–348 (2017).
296. J. Li, H. Lee, and K. J. Vahala, "Microwave synthesizer using an on-chip Brillouin oscillator," Nat. Commun. **4**, 2097 (2013).
297. K. J. Vahala, "Back-action limit of linewidth in an optomechanical oscillator," Phys. Rev. A **78**, 023832 (2008).
298. B. Morrison, A. Casas-Bedoya, G. Ren, K. Vu, Y. Liu, A. Zarifi, T. G. Nguyen, D.-Y. Choi, D. Marpaung, S. J. Madden, A. Mitchell, and

B. J. Eggleton, “Compact Brillouin devices through hybrid integration on silicon,” Optica **4**, 847–854 (2017).

299. N. T. Otterstrom, R. O. Behunin, E. A. Kittlaus, Z. Wang, and P. T. Rakich, “A silicon Brillouin laser,” Science **360**, 1113–1116 (2018).
300. T. Kippenberg, H. Rokhsari, T. Carmon, A. Scherer, and K. Vahala, “Analysis of radiation-pressure induced mechanical oscillation of an optical microcavity,” Phys. Rev. Lett. **95**, 1–4 (2005).
301. I. S. Grudinin, H. Lee, O. Painter, and K. J. Vahala, “Phonon laser action in a tunable two-level system,” Phys. Rev. Lett. **104**, 083901 (2010).
302. W. C. Jiang, X. Lu, J. Zhang, and Q. Lin, “High-frequency silicon optomechanical oscillator with an ultralow threshold,” Opt. Express **20**, 15991–15996 (2012).
303. L. Fan, C.-L. Zou, M. Poot, R. Cheng, X. Guo, X. Han, and H. X. Tang, “Integrated optomechanical single-photon frequency shifter,” Nat. Photonics **10**, 766–770 (2016).
304. H. Li, S. A. Tadesse, Q. Liu, and M. Li, “Nanophotonic cavity optomechanics with propagating acoustic waves at frequencies up to 12 GHz,” Optica **2**, 826–831 (2015).
305. C. L. Zou, X. Han, L. Jiang, and H. X. Tang, “Cavity piezomechanical strong coupling and frequency conversion on an aluminum nitride chip,” Phys. Rev. A **94**, 013812 (2016).
306. D. E. Chang, A. H. Safavi-Naeini, M. Hafezi, and O. Painter, “Slowing and stopping light with an optomechanical crystal array,” New J. Physics **1291**, 13–17 (2010).
307. M. Zhang, G. S. Wiederhecker, S. Manipatruni, A. Barnard, P. McEuen, and M. Lipson, “Synchronization of micromechanical oscillators using light,” Phys. Rev. Lett. **109**, 233906 (2012).
308. H. Pfeifer, T. Paraïso, L. Zang, and O. Painter, “Design of tunable GHz-frequency optomechanical crystal resonators,” Opt. Express **24**, 11407–11419 (2016).
309. M. Borselli, T. J. Johnson, and O. Painter, “Measuring the role of surface chemistry in silicon microphotonics,” Appl. Phys. Lett. **88**, 131114 (2006).
310. T. Asano, Y. Ochi, Y. Takahashi, K. Kishimoto, and S. Noda, “Photonic crystal nanocavity with a Q factor exceeding eleven million,” Opt. Express **25**, 1769–1777 (2017).
311. L. Fan, X. Sun, C. Xiong, C. Schuck, and H. X. Tang, “Aluminum nitride piezo-acousto-photonic crystal nanocavity with high quality factors,” Appl. Phys. Lett. **102**, 153507 (2013).
312. H. Liang, R. Luo, Y. He, H. Jiang, and Q. Lin, “High-quality lithium niobate photonic crystal nanocavities,” Optica **4**, 1251–1258 (2017).
313. M. J. Burek, J. D. Cohen, S. M. Meenehan, N. El-Sawah, C. Chia, T. Ruelle, S. Meesala, J. Rochman, H. A. Atikian, M. Markham, D. J. Twitchen, M. D. Lukin, O. Painter, and M. Lončar, “Diamond optomechanical crystals,” Optica **3**, 1404–1411 (2016).
314. M. Mitchell, D. P. Lake, and P. E. Barclay, “Realizing Q > 300000 in diamond microdisks for optomechanics via etch optimization,” arXiv:1808.09883 (2018).
315. C. Dory, D. Vercruysse, K. Y. Yang, N. V. Sapra, A. E. Rugar, S. Sun, D. M. Lukin, A. Y. Piggott, J. L. Zhang, M. Radulaski, K. G. Lagoudakis, L. Su, and J. Vuckovic, “Optimized diamond quantum photonics,” arXiv:1812.02287 (2018).
316. G. Bahl, K. H. Kim, W. Lee, J. Liu, X. Fan, and T. Carmon, “Brillouin cavity optomechanics with microfluidic devices,” Nat. Commun. **4**, 1994 (2013).
317. A. Krause, M. Winger, T. Blasius, Q. Lin, and O. Painter, “A high-resolution microchip optomechanical accelerometer,” Nat. Photonics **6**, 768–772 (2012).
318. K. L. Ekinci, Y. T. Yang, and M. L. Roukes, “Ultimate limits to inertial mass sensing based upon nanoelectromechanical systems,” J. Appl. Phys. **95**, 2682–2689 (2004).
319. P. Tiebot, R. Van Laer, and D. Van Thourout, “Thermal tuning of Brillouin resonance in free standing silicon nanowire,” in *Conference on Lasers and Electro-Optics* (OSA, 2018), paper jW2A.35.
320. J.-C. Beugnot, T. Sylvestre, and H. Maillotte, “Guided acoustic wave Brillouin scattering in photonic crystal fibers,” Opt. Lett. **32**, 2006–2008 (2007).
321. J.-C. Beugnot, S. Lebrun, G. Pauliat, H. Maillotte, V. Laude, and T. Sylvestre, “Brillouin light scattering from surface acoustic waves in a subwavelength-diameter optical fibre,” Nat. Commun. **5**, 5242 (2014).
322. R. Cohen, Y. London, Y. Antman, and A. Zadok, “Brillouin optical correlation domain analysis with 4 millimeter resolution based on amplified spontaneous emission,” Opt. Express **22**, 12070–12078 (2014).
323. A. Zarifi, B. Stiller, M. Merklein, N. Li, K. Vu, D.-Y. Choi, P. Ma, S. J. Madden, and B. J. Eggleton, “Highly localized distributed Brillouin scattering response in a photonic integrated circuit,” APL Photon. **3**, 036101 (2018).